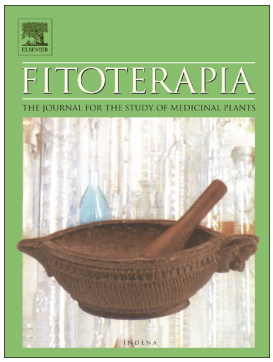
Journal Pre-proof



Comparative metabolomic profiling of Trichoderma cf. harzianum reveals cultivation-dependent chemical diversity under the OSMAC approach

Hadeel Almagthali, Joud Alshammari, Florbela Pereira, Isabelle S.R. Storer, Stefan Bidula, Mostafa E. Rateb, Arasu Ganesan, Amr El-Demerdash

PII: S0367-326X(26)00492-2

DOI: https://doi.org/10.1016/j.fitote.2026.107572

Reference: FITOTE 107572

To appear in: *Fitoterapia*

Received date: 5 July 2026

Revised date: 24 October 2026

Accepted date: 10 November 2026

Please cite this article as: H. Almagthali, J. Alshammari, F. Pereira, et al., Comparative metabolomic profiling of Trichoderma cf. harzianum reveals cultivation-dependent chemical diversity under the OSMAC approach, *Fitoterapia* (2026), https://doi.org/10.1016/j.fitote.2026.107572

This is a PDF of an article that has undergone enhancements after acceptance, such as the addition of a cover page and metadata, and formatting for readability. This version will undergo additional copyediting, typesetting and review before it is published in its final form. As such, this version is no longer the Accepted Manuscript, but it is not yet the definitive Version of Record; we are providing this early version to give early visibility of the article. Please note that Elsevier's sharing policy for the Published Journal Article applies to this version, see: https://www.elsevier.com/about/policies-and-standards/sharing#4-published-journal-article. Please also note that, during the production process, errors may be discovered which could affect the content, and all legal disclaimers that apply to the journal pertain.

© 2026 Published by Elsevier B.V.

Journal Pre-proof

Comparative Metabolomic Profiling of *Trichoderma cf. harzianum* Reveals Cultivation-Dependent Chemical Diversity Under the OSMAC Approach

Hadeel Almagthali [a, b], Joud Alshammari [a, c], Florbela Pereira [d], Isabelle SR Storer [a, h], Stefan Bidula [a, h], Mostafa E. Rateb[e], Arasu Ganesan [a] and Amr El-Demerdash* [a, f, g, h]

[a]School of Chemistry, Pharmacy and Pharmacology, University of East Anglia, Norwich Research Park, Norwich NR4 7TJ, United Kingdom.

[b]Department of Pharmacognosy, College of Pharmacy, Taif University, Al-Haweiah 21974, Saudi Arabia.

[c]Department of Pharmacognosy, College of Pharmacy, Jouf University, Sakaka, Aljouf 72341, Saudi Arabia.

[d]LAQV-REQUIMTE, Department of Chemistry, NOVA School of Science and Technology, Universidade Nova de Lisboa, 2829-516 Caparica, Portugal.

[e]Natural and Medical Sciences Research Centre, University of Nizwa, P.O. Box 33, Birkat Al Mauz, Nizwa, Oman

[f]Division of Organic Chemistry, Department of Chemistry, Faculty of Sciences, Mansoura University, Mansoura-35516, Egypt

[g]Department of Biochemistry and Metabolism, The John Innes Centre, Norwich Research Park, Norwich NR4 7UH, United Kingdom

[h]Centre for Microbial Interactions, Norwich Research Park, Norwich NR4 7UG, United Kingdom

***Corresponding author:** Amr El-Demerdash (A.E-D), School of Chemistry, Pharmacy and Pharmacology, University of East Anglia, Norwich Research Park, Norwich NR4 7TJ, United Kingdom. A.Eldemerdash@uea.ac.uk

Journal Pre-proof

Journal Pre-proof

Abstract: The one-strain many compounds (OSMAC) approach is an effective technique for promoting the production of bioactive secondary metabolites by activating cryptic gene clusters in microorganisms. This study aims to assess the effect of the OSMAC approach on the production of bioactive secondary metabolites of the freshwater-derived fungus *Trichoderma cf. harzianum*. Ethyl acetate extracts obtained from 10 different cultures were analysed using liquid chromatography coupled with high-resolution mass spectrometry (Q-Tof-LC-HR-MS), followed by complementary analytical techniques, including dereplication, multivariate analysis, and molecular networking. A total of 130 features were detected across the tested culture conditions according to Metabolomics Standards Initiative levels 2-4, of which 31 features were annotated only at the molecular formula level. Selected extracts exhibited moderate antimicrobial activity, particularly against *Staphylococcus aureu*s and *Candidozyma auris*. Molecular docking of major putatively annotated metabolites predicted favourable binding interactions with bacterial and fungal dihydrofolate reductase (DHFR) and bacterial DNA gyrase B (GyrB). These findings demonstrate that OSMAC-driven cultivation enhances chemical diversity and supports the discovery of bioactive metabolites from *T. cf. harzianum.*

Keywords: Fungal natural products, *Trichoderma harzianum*, OSMAC, secondary metabolites, LC-MS, GNPS, metabolomics, antimicrobial, molecular docking.

Journal Pre-proof

1. Introduction

Microbial natural products (MNPs) are low-molecular-weight organic compounds biosynthesised by microorganisms, including bacteria and fungi. The majority of natural products are secondary metabolites, which are generally described as molecules not critical for the survival of the producing organism but aid in enhancing its competitiveness [1]. They play essential roles as intracellular signalling molecules, providing a survival advantage in response to environmental pressures and during resource competition. Numerous secondary metabolites have been used as potent pharmacological agents; for instance, the majority of antibiotics are derived from microbial natural products [2].

These secondary metabolites are the result of dedicated biosynthetic machinery encoded within the producer's genome. The related genes are often grouped into biosynthetic gene clusters (BGCs). Genome sequencing has shown that microbes usually harbour various "cryptic" BGCs, which are not associated with chemically characterised molecules. These BGCs remain silent under standard laboratory culturing conditions [3]. Activating these cryptic BGCs is therefore essential for unlocking new chemical diversity of both pharmacological and biotechnological interest [3]. Therefore, genetic and cultivation-based methods have been assembled to promote the expression of these "cryptic" genes.

The one strain many compounds (OSMAC) approach addresses this challenge by altering cultivation conditions to stimulate the production of different metabolites from a single organism [4]. Zeeck and colleagues initially conceptualised the framework of the OSMAC approach. The fundamental concept behind this method is that each microbial strain has the possibility to synthesise numerous compounds, but only subsets of these compounds are produced under specific fermentation conditions. Consequently, variations in cultivation properties can stimulate the production and discovery of unique secondary metabolites [5]. By altering fermentation parameters such as temperature, salinity, aeration, and even the shape of the flasks, Zeeck and colleagues demonstrated that the fungus *Aspergillus ochraceus*, previously thought to produce only the metabolite aspinonene, was capable of producing 15 additional metabolites [5].

Trichoderma harzianum is a biocontrol fungus isolated from both marine and terrestrial environments. *T. harzianum* has the potential to produce a wide variety of biologically active secondary metabolites [6]. These metabolites have exhibited antifungal activity [7], cytotoxicity [8], and antimicrobial effects [9]. However, whole-genome sequencing of *T. cf. harzianum* unveiled many genes for the biosynthesis of compounds that were cryptic when cultured under standard conditions and considered an untapped source of bioactive compounds [10].

According to data submitted to the Central Asian and European Surveillance of Antimicrobial Resistance (CAESAR) network in 2023 by 15 countries, the majority of isolates (72%) reported in the recent surveillance of antimicrobial resistance in Europe were *Escherichia coli* (40%), *Staphylococcus aureus* (17%) and *Klebsiella pneumoniae* (15%)[11]. Furthermore, European surveillance reported that cases of *Candidozyma auris (*formerly *Candida auris)* infection continue to rise rapidly. This accelerated response is partly due to its ability to rapidly develop resistance mechanisms, including target modification and metabolic pathway flexibility [12].

Journal Pre-proof

These rising resistance trends highlight the urgent need to identify new molecular targets and develop alternative antimicrobial therapies. Dihydrofolate reductase (DHFR), a key enzyme in the folic acid biosynthesis pathway, plays a critical role in nucleotide production and cell proliferation. Consequently, inhibition of DHFR can disrupt DNA synthesis and lead to microbial cell death, making it an attractive therapeutic target [13, 14]. Similarly, the function of DNA gyrase (Gyr), a type II topoisomerase unique to bacteria, is responsible for introducing negative supercoils into DNA, a process essential for DNA replication and transcription. Inhibition of DNA gyrase disrupts DNA topology and ultimately leads to cell death [15, 16]. Importantly, the absence of DNA gyrase in human cells enhances its value as a selective pharmacological target for antibacterial drug development [15].

Metabolomics has emerged as a powerful platform for evaluating complex crude extracts and identifying marker metabolites [17]. When combined with the OSMAC approach, it provides a comprehensive and systematic tool to explore the chemical space developed under different cultivation conditions [18]. Metabolomic analysis relies on advanced analytical techniques, such as high-resolution mass spectrometry (HRMS) and nuclear magnetic resonance (NMR), to completely characterise the chemical diversity of metabolites within a given crude extract [19].

This study aimed to compare the metabolomic profiles of *T. cf. harzianum* cultured under ten different fermentation conditions. A complementary metabolomics analysis, combining multivariate analysis, Global Natural Product Social Molecular Network GNPS, and a dereplication strategy, was integrated to analyse the LC-MS/MS data from the different culture extracts. The biological relevance of these metabolites was then assessed through antimicrobial screening against bacterial (methicillin-resistant *Staphylococcus aureus* (MRSA), *S. aureus*, *Pseudomonas aeruginosa*, and *E. coli)* and fungal (*Aspergillus fumigatus*, *A. flavus*, *Candida albicans*, and *C. auris*) pathogens. Finally, molecular docking studies were performed on the eleven major putatively annotated compounds identified in the active extracts against bacterial DHFR, DNA gyrase B (GyrB), and fungal DHFR.

2. Materials and methods

2.1. Sample collection

The *T. cf. harzianum* strain used in this study was isolated from water sediments collected from the University of East Anglia Lake (52.6217° N, 1.2361° E) in Norwich, United Kingdom, in August 2022 (**Fig. S1**). The samples were serially diluted with sterile water and transferred to a potato dextrose agar (PDA) plate, which was then incubated at 28 °C for 2 weeks. To obtain pure isolates, fungal colonies were sub-cultured onto new PDA plates, and the pure cultures were preserved in 30% glycerol suspensions at -80 °C.

2.2. Identification of fungal strain

Journal Pre-proof

Taxonomic identification of the isolated fungal strain was achieved based on the nuclear ribosomal internal transcribed spacer (ITS) region together with the translation elongation factor 1-alpha (TEF1-α) locus. The ITS region is commonly accepted as a universal barcode sequence for fungi, although additional loci are often required for species-level resolution within the *Trichoderma harzianum* species complex [20, 21]. Briefly, conidia from a 7-day-old culture grown on PDA at 28 °C were suspended in cetyltrimethylammonium bromide (CTAB) buffer (BioChemica) and homogenised for 90 s using 0.5 mm glass beads in a bead beater. DNA was separated using chloroform, then precipitated from the organic phase with isopropanol, followed by washing with 70% ethanol. DNA was reconstituted in water, and the concentration was quantified using a Nanodrop 1000 (Thermo Fisher Scientific) [22]. PCR amplification was conducted with primers ITS1 (TCCGTAGGTGAACCTGCGG) and ITS4 (TCCTCCGCTTA TTGATATGC) for the ITS region, and EF1-728F (CATCGAGAAGTTCGAGAAGG) and EF1-986R (TACTTGAAGGAACCCTTACC) for the TEF1-α region (Thermo Fisher Scientific) and Phusion Flash polymerase (Thermo Fisher Scientific) according to the manufacturer's instructions [23]. PCR products were verified by gel electrophoresis. Amplicons were purified using PureLink Quick PCR Purification Kit (Invitrogen) and submitted to Eurofins Scientific for Sanger sequencing. Consensus sequences were analysed using BLASTn searches against the GenBank database (National Centre for Biotechnology Information, NCBI; https://blast.ncbi.nlm.nih.gov/Blast.cgi). ITS analysis showed the highest similarity to *Trichoderma harzianum* (99.42%; E-value = 2e−173). TEF1-α sequence analysis also showed the highest similarity to *Trichoderma harzianum* (95.07%; E value = 8e−118) but showed close similarity to related taxa, including *T. atrobrunneum* and *T. afroharzianum*. Accordingly, the isolate was conservatively designated as a member of the *T. harzianum* species complex (*Trichoderma cf. harzianum*) [24].

2.3. Fungal fermentation and extract preparation

To investigate the metabolic diversification of *T. cf. harzianum*, an OSMAC approach was applied by altering the composition of the selected culture medium and the incubation period. Ten different media were used, including both agar-based and rice-based media. The agar-based media included oatmeal agar (OAT), tryptone soy agar (TSA), PDA, Czapek-Dox agar (CZA), yeast malt glucose agar (YMG), and yeast malt glucose agar with amino acids (*L*-threonine, *L*-methionine and *L*-tryptophan) (YMG-aa). In contrast, rice-based media included rice grains (RM) and rice grains containing different salts, NaCl, NaBr, or $(NH_4)_2SO_4$. Culture media compositions are listed in (**Table S1**).

T. cf. harzianum was inoculated into three plates (90 mm in diameter) for each medium at 28 ± 2°C for 14 days for OTA, TSA, YMG, and YMG-aa. While the PDA medium was inoculated for 21 days, the CZA was inoculated for 30 days. On rice-based media, fungi were inoculated into three 250 mL Erlenmeyer flasks at 28 ± 2°C for 14 days (**Fig. S2**). Control cultures (blanks) were prepared under similar conditions, but without inoculating the fungus. After fermentation, each biological replicate was extracted independently; the mycelium was sliced into small pieces with a flat spatula and transferred into 250 mL glass Duran® bottles. Then, 3 × 50 mL of EtOAc was added and sonicated for 30 min at room temperature. The combined EtOAc phase was partitioned against Milli-Q water (150 mL)

to remove salts and water-soluble compounds. The organic extracts were dried over magnesium anhydrous sulphate and evaporated under reduced pressure. The resulting organic extracts were labelled 1–3 to represent three independent biological replicates (n = 3) for each cultivation condition, while uninoculated medium extracts were labelled C as controls. Each biological replicate was analysed separately by LC-MS/MS using a single injection, and all three replicates were retained as independent observations throughout subsequent statistical analyses. No technical replicate injections were performed.

2.4. Chemical analysis

2.5. HPLC profiles of the crude extracts

All extracts were analysed using an Agilent 1200 High-Performance Liquid Chromatography (HPLC). The analytes were separated using a reversed-phase HPLC (Kinetex 2.6 μm XB-C18 100 Å, LC Column 50 x 2.1 mm EA). A standardisation of 1 mg of each extract was solubilised in 1 mL of MeOH and filtered through a 0.2 μm syringe filter. A gradient solvent system of Milli-Q water (phase A) and acetonitrile (HPLC grade) (phase B), acidified with 0.1% formic acid, was used. A linear gradient was optimised: 0-2 min, 2% B; 2-25 min, 2-100% B; 25-28 min, 100% B, followed by equilibration with 2% B. The flow rate was 0.3 mL/min, and the injection volume was 2μL.

2.6. LC-MS analysis of crude extracts

T. cf. harzianum EtOAc extracts were subjected to ultra-high-performance liquid chromatography–quadrupole time-of-flight mass spectrometry, Agilent 6546 LC/Q-TOF (The John Innes Centre, Norwich Research Park). Instrument fitted with a reversed-phase column (Kinetex 2.6 μm XB-C18 100 Å, LC Column 50 x 2.1 mm EA). A binary solvent mixture consisting of 0.1% formic acid in Milli-Q water (phase A) and 0.1% formic acid in acetonitrile (phase B) was used at a constant flow rate of 0.3 mL/min and a total run time of 30 min. A linear gradient was optimised: 0-2 min, 2% B; 2-25 min, 2-100% B; 25-28 min, 100% B, followed by equilibration with 2% B. The flow rate was 0.3 mL/min. The instrument was operated in positive electrospray ionisation (HR-ESI+ve) mode. Reference parameters were selected: gas temperature at 325 °C, source voltage at 3500 V, and sheath gas flow rate at 12 L/min. MS scans were used in full-scan mode from *m/z* 100 to 1700. The calibration solution contains two internal reference masses at (*m/z* 121.050873 and *m/z* 922.0098). A permanent MS/MS exclusion list criterion was installed to control oversampling of the interior calibrant. As LC-MS acquisition was conducted solely in positive ionisation mode, only ionisable metabolites were detected; therefore, all downstream annotations and comparative analyses reflect a subset rather than the full complement of metabolites present in the extracts. Samples were injected in a non-randomised order, with biological triplicates grouped based on cultivation condition. Medium and solvent blanks

were included in the analytical sequence; however, pooled quality control (QC) samples were not prepared or injected. Therefore, systematic assessment of instrumental signal drift and QC-based analytical variability was not performed.

2.7. Dereplication of known compounds

Dereplication is a widely used strategy in natural product research to prioritise the isolation of novel compounds while quickly identifying known ones. It works by comparing LC-MS/MS profiles of crude extracts against spectral data from previously characterised secondary metabolites in natural product databases [25]. In the current study, dereplication analysis was performed through a combination of manual and computational approaches. Initially, an *in silico* dereplication was performed using SIRIUS 6, which predicts molecular formulas and fragmentation trees and predicts candidate molecular structures [26]. Then, the observed *m/z* ion peaks, fragmentation patterns, and adduct types were compared against two chemical databases, the Natural Products Atlas and REAXYS, to identify matches with previously reported compounds [27, 28]. Processed MS/MS data of *T. cf. harzianum* crude extracts were exported in mascot generic (.mgf) formats and uploaded into SIRIUS 6 for compound annotation. The molecular formula identification selected parameters included the following possible adducts ($[M+H]^+$, $[M+Na]^+$, $[M+ACN+H]^+$, and $[M+K]^+$), the permitted elements (H, C, N, O, P, S, Cl, and Br), and a structure database search applied to all applicable databases. During manual review of the LC-MS features, potential isotopic peaks, alternative adducts, and in-source fragments to minimise duplicate metabolite assignments were considered. All annotated compounds were classified based on the Metabolomics Standards Initiative confidence levels; no Level 1 annotations were assembled in this study, where compounds with library-matched MS/MS spectra by SIRIUS molecular formula assignment with SIRIUS Score ≥ 50%, CSI: FingerID structural candidate identification were classified to level 2, whereas features supported by diagnostic MS/MS fragmentation patterns or compound-class similarities, including those with multiple plausible structural candidates that could not be distinguished using the available evidence, were conservatively assigned to MSI Level 3. Features identified only by molecular formula prediction were classified as level 4 [29]. The putative annotated metabolite diversity reported in this study reflects only metabolites detectable under the applied LC–MS positive-ionisation conditions. It should therefore be considered a partial representation of the extracts' overall metabolome.

2.8. Data processing

The raw mass data files were converted to .mzXML format using the ProteoWizard MassConvert program [30]. These files were then processed using MZmine 4.3.0 to extract features from the raw data [31]. The major parameters for processing were as follows: retention time (0.50 to 26 min), max peaks in chromatogram 15, positive ion mode, and minimum feature height 2.0E5. The default or optimised parameters are used for high-resolution mass spectrometry data in each step. After feature detection and alignment, blank subtraction was performed, i.e. features detected in control media and solvent blanks were excluded from the final

data matrix to retain only fungal-derived metabolites. The detailed data-processing workflow and associated parameters are provided in (**Table S2**).The resulting peak list table was created and exported in comma-separated values (.csv) format for Multivariate analysis, while MS/MS spectral data were exported in (.mgf) format for compound annotation (SIRIUS) [26]. All LC-MS extract files were processed consistently to ensure comparability across various OSMAC conditions.

2.9. Multivariate data analysis

The MetaboAnalyst platform (https://www.metaboanalyst.ca/home.xhtml), accessed on March 28, 2026, is a web-based statistical analysis tool used for the extensive analysis of metabolomics data, interpretation, and integration with other omics data [32]. This investigation requires an input file containing the processed data files, including sample name, peak list (*m/z*), and peak intensities, exported as (.csv). Data files were subjected to normalisation by median and data scaling. Then, statistical analyses were employed, including unsupervised multivariate methods, such as principal component analysis (PCA), K-means clustering, hierarchical clustering, and dendrogram construction. The first two principal components (PC1 and PC2) were used to calculate Euclidean distances for PERMANOVA, with statistical significance assessed using 999 permutations. In addition, supervised partial least squares discriminant analysis (PLS-DA), data visualisation, and feature relationship analysis *via* a heatmap were employed [33]. Five-fold cross-validation was used for model validation with R^2, Q^2, and classification accuracy as performance metrics. Additionally, we assessed the statistical significance of class discrimination *via* permutation testing (100 permutations), using the separation distance (B/W) as the test statistic. Three biological replicates for each cultivation condition, resulting in balanced class sizes. All retained LC-MS features without prior ANOVA-based feature selection were used to perform PLS-DA. Variable importance in projection (VIP) scores were computed after model construction and used to prioritise discriminative LC-MS metabolite features for interpretation. VIP-ranked features were subsequently cross-referenced with ANOVA results for downstream interpretation. One-way analysis of variance (ANOVA) with false discovery rate (FDR) correction was performed; *p*-values were adjusted for multiple testing using the Benjamini–Hochberg procedure, and features with adjusted $p < 0.05$ were considered statistically significant. Fisher's least significant difference (LSD) post-hoc test was used for pairwise comparisons between cultivation conditions. Effect sizes were calculated as eta-squared (η^2) to estimate the proportion of variance associated with cultivation conditions. ***Supplementary data*** **Table 1** summarises feature-level ANOVA results, including *F*-statistics, FDR, *p*-values, and effect sizes. Fisher's LSD post-hoc comparison results are presented in ***Supplementary data*** **Table 2.**

2.10. GNPS molecular networking

A molecular network was generated on the GNPS webpage (http://gnps.ucsd.edu), accessed on June 28, 2025. The converted files were uploaded to GNPS for molecular networking analysis; in this approach, MS^2 spectra are arranged in a network based on their similarity and compared against a reference database to identify possible known compounds in the extract [34]. The molecular network was developed using the following parameters: precursor and fragment ion mass

tolerances were set to 0.02 Da each. Advanced network options were set as follows: Minimum cosine score: 0.7; minimum matched fragment ion: 6; node TopK: 10; minimum cluster size: 2; maximum connected component size: 100. For advanced library search options, the minimum number of matching peaks is six, and the score threshold is 0.7. GNPS-generated molecular networks are visualised and analysed in a web browser or Cytoscape software [35]. The nodes (compounds) arising from the control media and the methanol solvent blank were excluded. All available GNPS public spectral libraries were used for spectral matching. All annotated nodes were assessed for cosine score, number of shared fragment ions, and precursor mass error in parts per million (ppm). The quality of the library match was also evaluated based on the GNPS library quality rating system (Gold, Silver, Bronze). Independent statistical dereplication was conducted on annotated nodes using the DEREPLICATOR+ tool *via* the GNPS2 platform [36]. DEREPLICATOR+ was run with the following parameters: precursor ion mass tolerance, 0.02 Da; fragment ion mass tolerance, 0.02 Da; fragmentation model, 2-1-3 maximum charge, 1; and minimum score to consider a peptide-spectrum match as significant, 4. Metabolite false discovery rate (FDR%) and score-filtered results, and compound identities were cross-validated against GNPS library annotations.

2.11. Antimicrobial activity of crude extracts

2.12. Antibacterial activity

The antibacterial activity of the crude extracts was evaluated using the disc diffusion test against a variety of pathogenic bacteria, including MRSA (NCTC® 13373), *S. aureus* (ATCC® 25923), *P. aeruginosa* (NCTC® 10662), and *E. coli* (NCTC® 10418). Microbial suspensions were standardised to 0.5 McFarland turbidity before inoculation. Mueller–Hinton agar plates were inoculated with the test organisms, and sterile discs loaded with 200 µg of crude extract dissolved in dimethyl sulfoxide (DMSO) were placed onto the inoculated surfaces. DMSO was used as the negative control, while ampicillin (30 µg/disc) served as the positive control for Gram-positive strains, and ciprofloxacin (30 µg/disc) was used as the positive control for Gram-negative strains. Plates were incubated at 37 °C for 24 h, after which the antimicrobial activity of the extracts was estimated [37].

2.12.1. Antifungal activity

The antifungal activity of the crude extracts was evaluated against a variety of pathogenic fungi, including *Aspergillus fumigatus* (A1160+), *A. flavus*(22M8001325), *Candida albicans* (SC5314), and *Candidozyma auris* (NCPF8985). Antifungal susceptibility assays were conducted according to adapted Clinical and Laboratory Standards Institute (CLSI) reference methods: M27Ed4 for *C. albicans and C. auris.* and M38Ed3 for *Aspergillus* spp. [38, 39]. Conidia or yeast were incubated with metabolites in RPMI-1640 growth medium buffered with 0.165 M MOPS (3-(N-morpholino) propanesulfonic acid) buffer (pH 7.0) at 37 °C for 24 h. Following

incubation, 10 μg/mL resazurin in PBS was added to each well and incubated for 24 h at 37 °C. The ability of metabolically active cells to convert resazurin to the fluorescent product resorufin was quantified with a CLARIOstar plate reader using an excitation wavelength of 530 nm and an emission wavelength of 590 nm. Metabolic activity was calculated as a percentage of the untreated control.

To exclude potential interference from the culture medium, control media (media without fungal growth) were subjected to the same extraction procedure as the fungal cultures and estimated under similar antimicrobial assay conditions.

2.13. Preparation of the protein structures and molecular docking (MDock)

The optimisation of the 3D structure of the eleven top putatively annotated compounds (**Fig. S13** and **Fig. S14**) and the six positive controls (propyl-DAP 2-methylprop-1-en-1-yl-dihydrophthalazine and methotrexate for bacterial DHFR, 4-methyl-5-[3-(methylsulfanyl)-1H-pyrazol-5-yl]-2-thiophen-2-yl-1,3-thiazole and prop-2-yn-1-yl {[5-(4-piperidin-1-yl-2-pyridin-3-yl-1,3-thiazol-5-yl)-1H-pyrazol-3-yl]methyl}carbamate for GyrB, and 5-(4-chlorophenyl)-6,6-dimethyl-1,4-dihydro-1,3,5-triazine-2,4-diamine and 5-[(3*R*)-3-(5-methoxy-4'-methylbiphenyl-3-yl)but-1-yn-1-yl]-6-methylpyrimidine-2,4-diamine for fungal DHFR) was performed with the RDKit software [40] using the Experimental-Torsion Distance Geometry (ETDG) method [41]. The OpenBabel software (version 2.3.1) [42] was used to convert the mol2 files to PDBQT files. The 3D X-ray crystal structures of two bacterial DHFRs, *S. aureus* DHFR (*sa*DHFR) and *E. coli* DHFR (*ec*DHFR), were retrieved from the Protein Data Bank, PDB IDs 4FGG and 1RG7, respectively. The 3D X-ray crystal structures of two bacterial GyrB, *sa*GyrB and *ec*GyrB, were retrieved from the Protein Data Bank, PDB ID: 3G75 and 3G7E, respectively. The 3D X-ray crystal structures of two fungal DHFRs, *C. auris* (*ca*DHFR) and *C. albicans* (*cal*DHFR), were retrieved from the Protein Data Bank, PDB ID: 8CRH and 4H97, respectively. PDBQT files were used for docking to DHFR (4FGG, 1RG7, 8CRH and 4H97) and GyrB (3G75 and 3G7E) with AutoDock Vina (version 1.2.3) [43, 44]. Ions and ligands were removed from DHFR (4FGG, 1RG7, 8CRH and 4H97) and GyrB (3G75 and 3G7E) prior to docking using the AutoDockTools (http://mgltools.scripps.edu, accessed in February 2026). The search space coordinates were as follows: centre – X: -8.211, Y: 35.255, Z: -4.750 for 4FGG; X: 0.448, Y: 0.747, Z: 0.348 for 1RG7; X: 50.622, Y: -4.272, Z: 18.108 for 3G75; X: 38.588, Y: 12.742, Z: 22.715 for 3G7E; X: -8.309, Y: 17.812, Z: 77.062 for 8CRH; and X: 14.087, Y: 47.27, Z: -2.655 for 4H97. The dimensions were X: 20.000, Y: 20.000, Z: 20.000 for 4FGG, 3G75, 3G7E, 8CRH and 4H97, and X: 60.000, Y: 60.000, Z: 60.000 for 1RG7. Ligand tethering of the DHFR and GyrB was performed by regulating the genetic algorithm (GA) parameters, using 10 runs of the GA criteria. The docking binding poses were visualised with PyMOL Molecular Graphics System, Version 2.0 Schrödinger, LL, UCSF Chimera,[45] and Protein Ligand Interaction Profiler (PLIP) webtool [46]. The physicochemical properties, pharmacokinetic profiles, and toxicity profiles of the eleven top putatively annotated compounds (**Fig. S13** and **Fig. S14**) and the six positive controls were calculated using the Deep-PK online [47] webtool (https://biosig.lab.uq.edu.au/deeppk/, accessed in February 2026). The Deep-

PK tool encompasses several properties, including general physicochemical descriptors, absorption, distribution, metabolism, excretion, and toxicity-related endpoints. The complete list of predicted physicochemical, pharmacokinetic, and toxicity parameters is presented in the ***Supplementary data***.

3. Results and discussion

3.1. HPLC profiles of the crude extracts

Chromatographic analysis of the crude extracts obtained from the OSMAC technique revealed substantial variation in metabolite profiles across different cultivation conditions, confirming the strong influence of media composition on secondary metabolism (**Fig. 1**). Within the agar-based medium, the YMG supplemented with amino acid extract (YMG-aa) resulted in the appearance of several early-eluting peaks (5–10 min), indicating the induction of polar compounds. In contrast, the YMG extract exhibited four prominent peaks from 8 to 25 minutes. The TSA extract exhibited early eluting peaks (4-7 min). The PDA extract showed several major peaks from 7 to 25 min. Whereas CZA and OAT extracts resulted in relatively simple chromatographic patterns with few prominent peaks. In addition, the rice media supplemented with salt showed different metabolite profiles. The salt-supplement extract developed unique peaks not detected in the rice media extract alone. The addition of ammonium sulphate to the culture media increased peak numbers and intensities, particularly between 8 and 25 minutes, suggesting altered metabolite production under this cultivation condition. Rice medium supplemented with sodium chloride or sodium bromide extracts exhibited major peaks between 10 and 13 minutes. These variations may reflect cultivation-dependent changes in secondary metabolite biosynthesis; however, the underlying biochemical mechanisms remain unknown. This chemical analysis offers an initial exploration of the diversity of specialised metabolites produced by *T. cf. harzianum*. The strain-generated compounds span a range of polarities, with retention times between 3 and 26 minutes. Importantly, the choice of fermentation conditions had a clear impact not only on which metabolites were present but also on their relative abundances. This aligns with the principles of the OSMAC approach, whereby variations in fermentation medium composition and incubation duration can influence fungal secondary metabolite production, potentially promoting the expression of metabolites that remain undetected under standard cultivation conditions.

3.2. Dereplication of known compounds

Dereplication analysis showed significant metabolic differences among *T. cf. harzianum* EtOAc extracts, supporting the OSMAC approach's effectiveness in enhancing chemical diversity. A total of 130 LC-MS features were putatively annotated using SIRIUS based on MSI confidence levels. No features were confirmed as compounds (Level 1) because no authentic chemical standards or purified isolates were available. Most features were annotated at MSI levels 2 and 3, whereas 31 features could only be assigned at the molecular formula level (level 4). ***Supplementary data*** **Table 3**. The putatively annotated metabolites were grouped into peptides, alkaloids, terpenoids, polyketides, fatty acids, and other natural product classes.

When the extracts were classified into two distinct groups based on the cultivation media used, clear differences emerged between agar- and rice-based media, indicating that substrate type strongly affected fungal metabolite expression. Agar-based media were dominated by alkaloids (39%), followed by polyketides (24%) and peptides (21%), whereas terpenoids were present only in low abundance (3%). In contrast, rice-based media revealed a markedly distinct chemical profile, with polyketides (28%) and terpenoids (27%) illustrating the predominant classes, while alkaloids decreased substantially to 15%. Fatty acids were also more abundant in rice-based cultures (14%) than in agar-based cultures (9%) (**Fig. 2-a**). These variations indicate that rice-based substrates provide nutritional and environmental conditions that favour activation of biosynthetic pathways associated with polyketide and terpenoid production. In comparison, agar-based conditions may preferentially support nitrogen-associated alkaloid biosynthesis.

Additional variation in metabolite distribution was observed, confirming that specific medium composition and incubation duration affect secondary metabolite production. YMG-aa extracts displayed the highest abundance of alkaloid-related metabolites (72%), indicating induction of nitrogen-containing secondary metabolites under this condition, while other classes were detected in minor amounts. In comparison, polyketides are the dominant class in YMG, PDA, and OAT, suggesting induction of polyketide synthase-related pathways. In the TSA extract, alkaloids and peptides are the most prominent classes of tentatively annotated compounds, with 36% for each. Whereas alkaloids and terpenoid-related metabolites characterised the CZA extract, accounting for 22% each. (**Fig. 2-b**). Conversely, the terpenoid and polyketide classes are the most abundant related metabolites in a rice-based medium. Rice extract showed a high percentage of terpenoids (33%), followed by polyketides (24%) and fatty acids (19%). Indeed, the metabolic profiles are influenced by the addition of salt to rice cultivation media. RM-NaCl is characterised by a high representation of polyketides (33%) and terpenoids (26%); similarly, RM-NaBr is dominated by polyketides (31%) and terpenoids (27%). In contrast, RM-$(NH_4)2SO_4$ is mainly composed of terpenoids (26%), with polyketides and peptides accounting for 22% each (**Fig. 2-b**). These findings highlight that differences in incubation duration and nutrient composition among media, in which carbon and nitrogen availability may influence the activation of distinct biosynthetic pathways, thereby altering secondary metabolite production.

3.3. *Multivariate data analysis*

Metabolic profiles of the *T. cf. harzianum* fungi cultivated based on the OSMAC strategy were conducted by LC-MS using electrospray ionisation in positive mode. With LC-MS, variations in the metabolic profile of extracts can be visually described. To display the metabolomic differences between various extracts, multivariate analyses were performed. The most practically employed multivariate test used to minimise the dispersity of datasets is the unsupervised method [48]. The two-dimensional PCA score plot enabled the assessment and grouping of samples based on their metabolic profile similarities and differences. The resulting PCA revealed five components (PCs 1-5) that explain 82.2% of the total variation. The first two principal components explained 56.8% of the total variance, with PC1 accounting for 35.8% and PC2 accounting for 21.0%. Additionally, in the 2D score plot (**Fig. 3a**), a clear separation was observed among the extracts,

with minimal overlap between groups and distinct clustering of biological replicates within each medium, showing similarity among biological replicates. Rice-based media extracts were clustered in the same area, whereas YMG and YMG-aa extracts were well-separated clusters along the PC1 and PC2 axes. This indicated that adding amino acids to the media was associated with differences in the metabolomic profile.

Furthermore, TSA and other groups, including PDA, CZA, and OAT, exhibited distinct chemical profiles that were significantly clustered apart from those on rice-based media. The closed clustering pattern, unlike group separations, indicated that media composition significantly influenced the metabolic profile of the fungus. This result was supported by the PERMANOVA value (pseudo-F = 271.49, R^2 = 0.99188, p = 0.001). However, multivariate dispersion was not independently assessed; therefore, differences in within-group variability cannot be excluded as contributing to the observed significance.

To evaluate the similarity between different media extracts based on metabolic variation, a hierarchical clustering dendrogram was used. Samples were grouped into two major clusters based on the type of media used (agar-based or rice-based) (**Fig. 3b**). The first cluster, which was rice-based, was divided into two levels. The first level was RM-$(NH_4)_2SO_4$, and the second level consisted of two groups: Group 1, RM, and Group 2 (RM-NaBr and RM-NaCl). The second cluster was agar-based media, which was divided into two levels. The first level contains YMG-aa and TSA, while the second level consists of two groups: Group 1 (CZA and PDA) and Group 2 (OAT and YMG). A distinct separation between media was observed, showing that cultivation conditions strongly affect metabolite composition. K-means clustering revealed differential clustering of extracts into three major clusters, reflecting distinct metabolic responses to cultivation media. (**Fig. 3c**). Based on metabolic variation, the separation patterns were closely aligned with those of the PCA analysis. This clustering supports the PCA and dendrogram results by showing that samples with similar principal component scores also have similar chemical compositions, confirming the influence of culture medium on metabolite profiles.

Regarding the PLS-DA, a supervised multivariate analysis was carried out in order to assess further metabolic differences. The score plot (**Fig. 3d**) showed clear separation among extracts grown in different cultivation conditions, with components **1** and **2** accounting for 29.7% and 24.3% of the modelled variation, respectively. The five-fold cross-validation improved across models. The third component had the highest explanatory and predictive values ($R^2 \approx 0.892$ and $Q^2 \approx 0.771$), with the classification accuracy of 0.304. This shows that, although the Q^2 value is favourable, the ability to correctly assign samples to their respective cultivation conditions remains limited. Permutation testing with 100 permutations showed that the observed class separation was significantly greater than that from randomly permuted datasets (empirical $p < 0.01$), suggesting the supervised discrimination was unlikely to arise by chance. Furthermore, 378 of 395 metabolite features were identified as statistically significant across cultivation conditions by one-way ANOVA with FDR correction. This result suggests that the cultivation conditions were associated with significant differences in LC-MS feature intensities. VIP-ranked metabolites selected for downstream interpretation were cross-checked against the ANOVA results, and only ANOVA-significant features were included in the subsequent interpretation. Overall, the PLS-DA

findings support cultivation-associated differences in LC-MS feature profiles, although the limited classification accuracy and small number of biological replicates per condition warrant cautious interpretation.

The VIP (Variable Importance in Projection) analysis is a widely used method in multivariate statistics, particularly in PLS-DA, for ranking variables by their contribution to the model. Features with VIP scores >1 are conventionally considered significant contributors to group discrimination [49]. In the current study, the VIP (**Fig. 3e**) was performed to identify the fifteen metabolites contributing most strongly to discrimination among fungal extracts cultivated in different media. These features were determined based on their *m/z* values and retention times and subsequently dereplicated using SIRIUS for molecular formula prediction. Putative formulas were assigned based on exact mass, RT, adduct type and error value. SIRIUS tentatively assigned the molecular formula for the feature summarised in (**Table 1**). Features lacking a reliable SIRIUS annotation or mass errors above 5 ppm were not assigned due to inadequate confidence in prediction. The associated heatmap showed that these metabolites varied consistently across media, supporting our finding that different growth parameters produce different metabolic profiles. Together, these outcomes indicate that the OSMAC strategy effectively enhances the chemical diversification of *T. cf. harzianum*.

To visualise the relative abundance of the top 25 metabolites across *T. cf. harzianum* extracts cultivated in various media, a heatmap (**Fig. 3f**) was generated using normalised and auto-scaled LC-MS data. The top 25 metabolites were selected based on ANOVA ranking and cross-checked for FDR-adjusted significance. Two major metabolite clusters were observed. One cluster revealed relatively high abundance in TSA, YMG, and YMG-aa, whereas lower abundance was observed in rice-based media. The second cluster showed high abundance in PDA and rice-based media, suggesting selective induction of metabolite production under these conditions. Putative formulae for the 25 most significant features were assigned based on mass accuracy, RT, adduct type and corresponding mass errors (ppm). Only features showing acceptable mass accuracy, chemical formulas, and sufficient SIRIUS confidence were included for tentative dereplication. Dereplication details for the top 25 metabolites in the heatmap provided in (**Table 2)**. Biological replicates clustered closely within each medium, further confirming reproducibility of the LC-MS dataset. These abundance patterns supported the clustering observed in PCA, HCA, and K-means analyses.

Although different metabolic profiles were observed across cultivation conditions, pooled quality control (QC) samples and replicate injections of the same sample were not included in the LC-MS/MS analytical sequence. Therefore, instrumental signal drift, QC-based analytical variability, and injection repeatability could not be systematically evaluated. The non-randomised injection order may also have introduced analytical sequence effects that could be confounded with cultivation-dependent variation in metabolic profiles. These limitations should be considered when observing the metabolomic differences.

Overall, the statistical analyses and dereplication findings indicated that cultivation conditions have a strong, reproducible effect on fungal secondary metabolism, affecting both the global metabolomic structure and individual discriminative metabolites. The agreement across unsupervised, supervised, and univariate analyses supports the conclusion that medium optimisation is a critical determinant of metabolite diversification. Additionally, these outcomes revealed that the identified

metabolites varied across different media compositions. K-means clustering revealed differential clustering of extracts into three major clusters; agar-based media clustered into two distinct clusters (**Fig.3c**). The first cluster, comprising YMG-aa and TSA extracts, may reflect the presence of comparable putatively annotated metabolite classes, mainly alkaloids and peptides, detected in both extracts. Consistent with this observation, both extracts appeared at the same level in the dendrogram (**Fig. 3b**).

The second cluster, comprising OAT, YMG, PDA, and CZA extracts, also showed close similarity in the feature-based clustering analysis. In the dendrogram (**Fig. 3b**), OAT and YMG were clustered at the same level, suggesting the presence of similar putatively annotated polyketide and alkaloid features in both extracts. PDA and CZA extracts clustered at the same level, suggesting similar overall feature composition. This pattern may reflect overlapping putatively annotated metabolite classes: PDA is characterised mainly by polyketides and peptides, while CZA showed a more consistent distribution across alkaloids, peptides, polyketides, terpenoids, and fatty acids. Conversely, rice-based media revealed clustering in the third cluster in the K-means clustering test (**Fig. 3c**), which may be explained by the dominance of the terpenoid class. Adding salt to the media affected the metabolic profile; rice media supplemented with sodium chloride or sodium bromide extracts showed a high representation of polyketides and terpenoids. The dendrogram clustering (**Fig. 3b**) supports this finding; RM-NaCl and RM-NaBr clustered at the same level. In contrast, RM-$(NH_4)_2SO_4$ is primarily composed of terpenoids, peptides, and polyketides, and clustered at different levels.

3.4. GNPS molecular networking

To further investigate the metabolites of the ten different media extracts, LC-MS data were submitted to the GNPS workflow for molecular network structure. MS-based molecular networking links mass spectra of metabolites based on the similarity of their fragmentation patterns [50, 51]. The molecular networking analysis of extracts from different cultures revealed that variations in fermentation conditions influence secondary metabolite production. These conditions affected the number of nodes generated in the networks. The data were classified into two distinct networks based on the cultivation media used: **agar-based and rice-based** media. The network developed from agar-based media extracts comprised 1334 nodes, with 62% of the nodes organised into 24 major clusters (each containing more than 10 nodes) (**Fig. S3**). In comparison, rice-based media extracts yielded 607 nodes, with 73% of the nodes organised into 15 major clusters (**Fig. S4**). However, only selected nodes with supporting annotations were considered for interpretation.

Agar-based media extracts network revealed enormous clusters; notably, the third major cluster (**Fig. 4**) is peptaibol-type cyclic peptides centred on the node at *m/z* 1175.77, comprised multiple nodes including *m/z* 1189.78, 1445.01, 1459.02, 1471.02, 1473.04, and 1474.04, linked by high intra-cluster cosine similarity scores of 0.73–0.96, consisting of series cyclic peptide analogues varying amino acid substitutions. The node at *m/z* 1175.77 was putatively annotated as **trichorozin-II** through spectral library matching against bronze-quality library entries with a cosine score of 0.89, 20 shared fragment ions, and a precursor mass

error of 1 ppm (**Fig. S5**). DEREPLICATOR$^+$ putatively annotated **trichorozin-II** at cluster index (score = 24, FDR = 0.00%). In addition, SIRIUS 6 assigned the molecular formula of this node $C_{58}H_{102}N_{12}O_{13}$ $[M+H]^+$ with a SIRIUS score of 100% and a median mass error of -2.574 ppm. CSI: FingerID structural annotation yielded **trichorozin-II** as the third-ranked candidate alongside closely related *Trichoderma* cyclic peptides.

GNPS annotated the adjacent node at *m/z* 1189.78 *via* spectral library matching against bronze-quality library entries, with a cosine score of 0.79, 26 shared fragment ions, and a 2 ppm mass error, and putatively annotated it as **trichorozin-IV** (**Fig.S6**). DEREPLICATOR$^+$ putatively annotated this node as the peptaibol **trichorozin-IV** (score = 28, FDR = 0.00%). From SIRIUS, the molecular formula $C_{59}H_{104}N_{12}O_{13}$ $[M+H]^+$ was assigned with a SIRIUS score of 100% and a median mass error of 0.518 ppm, with **trichorozin-IV** returned as the second-ranked CSI: FingerID candidate. **Trichorozin-IV, with** molecular formula $C_{59}H_{104}N_{12}O_{13,}$ differs from that of **trichorozin-II** ($C_{58}H_{102}N_{12}O_{13}$) by exactly one methylene unit (CH_2, 14.016 Da), thereby establishing their homologous relationship. Both nodes are assigned MSI Level 2 confidence. Also, a node at *m/z* 1161.75 within this cluster has conflicting annotations between GNPS (**trichorovin-IIIb**, cosine = 0.73) and DEREPLICATOR$^+$ (**trichodermide E**, Score = 21, FDR = 0.00%), with low SIRIUS confidence and is therefore reported at MSI Level 3 ($C_{57}H_{100}N_{12}O_{13}$). Both belong to the *Trichoderma* peptide families.

The detection of trichorozin-II in the PDA and OAT, and trichorozin-IV in the PDA media extracts is biologically well-supported. Trichorozins are cyclic lipopeptides native to *Trichoderma* species, and their previous report from *T. harzianum* is compatible with the specified secondary metabolite repertoire of this genus [52]. Trichorozins exhibited voltage-dependent ion-channel-like activity in lipid bilayers [52].

The next spectral cluster in the agar-based media network (**Fig. 5**) formed from four nodes rising from the OAT extract at *m/z* 1111.69, 1112.70, 1125.71, and 1126.71, with high intra-cluster cosine similarity scores ranging from 0.72 to 0.93, indicating a series of structurally related analogues. GNPS spectral library matching against bronze-quality library entries with a cosine score of 0.88 and 30 shared fragment ions annotated the node at *m/z* 1125.71, placing this cluster within the **WLIP/Viscosin/Massetolide** cyclic lipopeptide molecular family, with a precursor mass error of 9 ppm, which is above the typical 5 ppm threshold and is noted as a limitation of this annotation. (**Fig. S7**). To further investigate the structural identity of this cluster, the LC-MS data were processed using SIRIUS 6 with CSI: FingerID structural annotation, which assigned the molecular formula $C_{54}H_{96}N_{10}O_{15}$ to the node at *m/z* 1125.71 $[M+H]^+$ with a SIRIUS score of 100%, 43 of 43 fragment ions explained, accounting for 80.3% of total spectral intensity, and a median mass error of -0.968 ppm. CSI: FingerID returned **pseudodesmin A** as the top structural candidate with a Tanimoto similarity of 83.17%, followed by **viscosinamide C** (81.67%), both cyclic lipodepsipeptides belonging to the viscosin family. The node at *m/z* 1111.69 was independently annotated by SIRIUS/CSI: FingerID as **pseudodesmin B** (molecular formula $C_{53}H_{94}N_{10}O_{15}$, Tanimoto similarity = 84.59%), a structural analogue differing from **pseudodesmin A** by a single methylene unit (14.02 Da) in the fatty acid chain, a relationship consistent with the high intra-cluster cosine similarity of 0.91 observed between these two nodes. ClassyFire chemical class prediction verified that both compounds are cyclic depsipeptides within the lipopeptide natural product superclass, with a posterior probability of 98.97%.

Journal Pre-proof

To additionally validate these findings, further *in silico* fragmentation analysis was performed using CFM-ID 4.0 against the **pseudodesmin A** structure illustrated substantially spectral coverage with the base peak at *m/z* 714.44 assigned as a cyclic depsipeptide ring fragment (score = 10.89), the second most abundant fragment ion at *m/z* 842.50 (relative intensity 92%) assigned as a complementary ring fragment (score = 10.44), and other fragment ions at *m/z* 256.23, 284.22, 314.21, 383.23, 412.28, 907.59, 925.57, and 1107.70 assigned as fatty acid chain and peptide sequence ions consistent with the **pseudodesmin A** scaffold, yielding around 15 major assigned peaks in total (**Fig. S8**). Also, independent validation utilising DEREPLICATOR$^+$ on the GNPS2 platform provided additional computational support for these candidate putative annotations: **pseudodesmin B** at *m/z* 1111.69 (score = 49, FDR = 0.00%) and **viscosinamide** at *m/z* 1125.71 (score = 47, FDR = 0.00%), both members of the viscosin cyclic lipopeptide family. Pseudodesmins A and B are cyclic lipodepsipeptides that were previously reported from a *Pseudomonas* [53]. Their annotation in *T. cf. harzianum* is unexpected, as the biosynthetic gene clusters responsible for pseudodesmin synthesis have not previously been reported in *Trichoderma* genomes.

Although computational annotation techniques are suggested for the same molecular family, these identifications should be interpreted as putative rather than definitive. The combined proof from GNPS molecular networking, GNPS spectral library matching, SIRIUS, DEREPLICATOR+, and CFM-ID consistently supports the assignment of these metabolites to a viscosin-like cyclic lipodepsipeptide molecular family. Nevertheless, the absence of authorised reports of pseudodesmin- or viscosinamide-type metabolites from *T. harzianum* complex fungi suggests that these metabolites may represent structurally related analogues rather than authentic reference compounds. Therefore, the suggested annotations are reported as MSI Level 3 annotations, remembering their assignment based on orthogonal computational evidence without the isolation of authentic standards. However, the convergence of multiple independent annotation tools provides strong evidence for the existence of previously unreported cyclic lipodepsipeptides in *T. cf. harzianum* extracts.

The **fusaperazine E** (**Fig. 5**) was putatively identified in molecular networks from both agar-based (YMG, CZA, OAT, and PDA) and rice-based media extracts. GNPS spectral library matching against bronze-quality library entries

annotated the node at *m/z* 361.156 with a cosine score of 0.87 and 8 shared fragment ions, putatively identifying the compound as **fusaperazine E**, with a precursor mass error of 5 ppm (**Fig. S9**). In SIRIUS 6, the molecular formula $C_{19}H_{24}N_2O_3S$ was assigned to this node $[M+H]^+$ with a Sirius Score of 97.357%, 42 of 53 fragment ions presented, and a median mass error of -3.653 ppm, establishing the exact monoisotopic mass of 360.149 Da corresponding to fusaperazine E. In addition, DEREPLICATOR$^+$ putatively identified this node with the SMILES for fusaperazine E (score = 7, FDR = 0.26%). Fusaperazines are 2,5-diketopiperazine alkaloids (DKPs), a structurally diverse class of cyclic dipeptide derivatives originally reported from *Fusarium* species, but related DKPs, such as gliotoxin, have been widely reported from *Trichoderma* and other ascomycete fungi [54, 55].

3.5. Antimicrobial activity

3.5.1. Antibacterial activity

Journal Pre-proof

To assess whether *T. cf. harzianum* extracts exhibit condition-dependent antibacterial activity, antibacterial susceptibility testing was performed against a range of human pathogens. Extracts obtained from cultures grown in YMG-aa and PDA showed antibacterial activity against *S. aureus*. The YMG-aa extract displayed the highest antibacterial activity, with an 18.85±0.49 mm zone of inhibition, followed by the PDA extract (10±1 mm). However, neither extract showed activity against the other bacteria tested (**Table S4, Fig. S10**). All other extracts did not inhibit the growth of any of the bacterial species assessed.

To confirm that this activity developed from fungal metabolites rather than from culture medium ingredients, extracts prepared from uninoculated control media YMG-aa and PDA were tested against *S. aureus* under similar conditions. No inhibitory action was observed, indicating that the antibacterial activity was associated with fungal-derived metabolites.

3.5.2. Antifungal activity

Extracts from cultures grown in RM-NaBr and RM-$(NH_4)_2SO_4$ media inhibited the growth of *C. auris*, with IC_{50} values of 35.85 µg/mL and 99.86 µg/mL, respectively. respectively. However, these extracts showed no activity against the other pathogenic fungi tested. Similarly, extracts obtained from YMG-aa, PDA, OAT, YMG, CZA, TSA, M, and RM-NaCl showed no antifungal activity against any of the fungal species assessed (**Fig. S11**). These results indicate that variation in fermentation conditions can significantly influence the production of bioactive metabolites in *T. cf. harzianum*. To verify that the observed activity was not attributable to the culture medium, an extract from RM-NaBr and RM$(NH_4)_2SO_4$ (uninoculated control medium) was assessed against *C. auris*. The control medium extract showed no activity, indicating that the antifungal activity was attributable to metabolites produced by the fungus (**Fig. S12**).

3.6. Molecular docking analysis of candidate metabolites against microbial targets

A combination of metabolomics and *in silico* approaches has enabled a shorter route to identifying bioactive natural products. Within this framework, the compounds selected for molecular docking were major putatively annotated metabolites detected in the active extracts and were evaluated as candidate contributors to the observed antimicrobial effects. Selection was based on prominent peaks observed in the chromatograms, which were consistent with the MS results, and on putative annotations from SIRIUS (Level 2 MSI), supported by accurate mass, molecular formula prediction, and MS/MS fragmentation patterns. These metabolites were not isolated or validated in biological tests. To provide preliminary insight into potential mechanisms underlying the antimicrobial activity observed in selected *T. cf. harzianum* extracts, molecular docking was performed against two well-established enzymatic targets [14, 15]. DHFR was selected as a broad microbial target, given its essential role in folate metabolism in both bacteria and fungi. In contrast, GyrB was included as a bacteria-specific target, as this type II topoisomerase is present only in prokaryotes and is widely exploited in antibacterial drug discovery. These targets were considered biologically relevant because several classes of natural products, including indole-, quinolone-, coumarin-, flavonoid- and polyphenol-like scaffolds, have previously been reported to interfere

with folate metabolism or DNA topology [14, 15]. Notably, the major annotated metabolites in our extracts contained structural motifs reminiscent of these compound families, providing a reasonable rationale for exploring potential interactions with DHFR and GyrB. Although no direct experimental evidence currently links the annotated metabolites to inhibition of either enzyme, the selection of DHFR and GyrB offers a meaningful starting point for hypothesis generation. Accordingly, the docking results should be interpreted as exploratory predictions, intended to guide future mechanistic studies rather than to establish definitive target engagement.

3.6.1. Molecular docking against bacterial targets

A molecular docking investigation was conducted for the top six putatively annotated compounds (**1-6**) in the (YMG-aa) and (PDA) extracts (**Fig. S13**) with bacterial DHFR, *sa*DHFR and *ec*DHFR and bacterial GyrB, *sa*GyrB and *ec*GyrB.

In the YMG-aa extract, the top three compounds were putatively annotated, including **indole-3-carboxaldehyde** (**1**), showing a relative peak intensity = 25.12%. It is an indole alkaloid reported from various natural sources, including plants, microorganisms, and marine organisms, emphasising its widespread occurrence [56-58]. It exhibits weak antibacterial activity against *S. aureus* and *E. coli*, with MIC values of 862.1 μM [59]. Additionally, exhibited selective cytotoxicity against prostate cancer cell lines PC-3M and lymph node carcinoma of the prostate (LNCaP), with IC_{50} values of 34.7 and 25.6 μM, respectively [60]. This compound was previously reported from *Trichoderma* sp.[61]. **Indole-3-acetic acid** (**2**) showed a relative peak intensity of 14.10%. This alkaloid was previously reported from *Trichoderma* strains, including *T. brevicompactum*, *T. gamsii*, and *T. harzianum*. The production of **2** is generally improved by adding tryptophan to the culture medium [62]. Further, Bader *et al*. emphasised that even without the addition of indole derivative compounds, *Trichoderma* produces indole-3-acetic acid [62]. To investigate the antibacterial effects of indole-3-acetic acid isolated from *Fusarium* sp., the following strains were tested: *Priestia megaterium*, *B. subtilis*, *C. perfringens*, *E. coli*, MRSA, and *S. aureus*. It shows weak activity against *P. megaterium* (285.7 μM) and is inactive against other strains (>571.4 μM) [63]. The third compound, putatively annotated as **tryptanthrin** (**3**), has a relative peak intensity of 4.27%. Compound **3**, an indoloquinazoline alkaloid, was reported from *Candida lipolytica* fungi and a variety of natural sources [64, 65]. It exhibits a variety of biological effects, including antibacterial, antifungal, antiprotozoal, and antiparasitic activities [65].

Whereas the high abundance peak in PDA with a relative intensity of 9.42% was putatively annotated as **harzianin HC XII** (**4**), which is a peptide that was previously isolated from *T. harzianum* strains (M-903614; M-903603), it displayed antibacterial effects against *S. aureus*, whereas it is inactive against *E. coli* [66]. The fifth annotated compound, **harzianolide** (**5**), with a relative intensity of 1.44%, is a butenolide that was previously isolated from *T. harzianum* and plays a role in plant growth regulation and plant defence responses [67]. Then, the sixth compound, ; putatively annotated as **fusaperazine E** (**6**), with a relative intensity of

1.29%, is a diketopiperazine derivative previously isolated from *P. crustosum* [54]. Compound **6** was assessed for antibacterial activity using the nematode *Caenorhabditis elegans* infected with the human opportunistic pathogen *Enterococcus faecalis*, showing no significant effect on nematode survival [54]. The results obtained from molecular docking performed with the use of AutoDock Vina software on DHFR and GyrB enzymes originating from bacteria are presented in **Table 3**.

The putatively annotated metabolites were selected as potential DHFR and GyrB binders based on docking predictions with the lowest calculated ΔG_B. Consequently, metabolites **3**, **4**, **5,** and **6** for both *sa*DHFR and *ec*DHFR showed the most favourable predicted binding affinities towards bacterial DHFR, with ΔG_B values below -6.7 kcal/mol (**Table 3**). In the case of GyrB, metabolites **3** and **5** for *sa*GyrB and **2**, **3**, **5** and **6** for *ec*GyrB were identified as having the most favourable predicted binding affinities towards bacterial GyrB, with a ΔG_B value lower than -6.3 kcal/mol (**Table 3**). Only antibacterial activity against *S. aureus* was observed for the (YMG-aa) and (PDA) extracts, with inhibition zones of 18.85 ± 0.49 mm and 10 ± 1 mm, respectively (**Table S3**). Furthermore, it has been established that **1**, **2**, and **3** are the putatively annotated metabolites with the highest relative LC-MS peak intensities in the YMG-aa extract, with percentages of 25.12, 14.10, and 4.27, respectively. Conversely, the PDA extract demonstrates a different metabolic profile, with the putatively annotated metabolites with the highest relative LC-MS peak intensities being **4**, **5**, and **6**, exhibiting percentages of 9.42, 1.44, and 1.29, respectively. These docking predictions and experimental antibacterial findings complement each other; however, a direct relationship between individual metabolites and extract activity has not been established.

Docking scores also predicted favourable binding to *E. coli* targets, although the corresponding extracts showed no measurable antibacterial activity against *E. coli*. The absence of detectable activity against *E. coli* compared with *S. aureus* may reflect differences in cell envelope architecture: *E. coli* is Gram-negative and possesses an outer membrane that restricts penetration of many natural products, potentially preventing compounds from accessing intracellular targets such as DHFR or GyrB, although this hypothesis was not experimentally investigated. The detailed docking interactions of the selected putatively annotated metabolites with favourable predicted binding interactions are shown in **Table 4** and **Fig. S13**. Of the metabolites reported in **Table 4**, only **3** and **5** were selected as the putatively annotated metabolites with favourable predicted binding interactions against both *sa*DHFR and *sa*GyrB. Features putatively assigned to these metabolites were detected in the YMG-aa and PDA extracts, respectively.

3.6.2. Molecular docking against fungal targets

A molecular docking investigation was conducted for the top five putatively annotated compounds (7-11) in the (RM-NaBr) and (RM-$(NH_4)_2SO_4$) extracts (**Fig. S14**) with fungal DHFR, *ca*DHFR and *cal*DHFR.

Journal Pre-proof

In the RM-NaBr extract, the top three compounds were putatively annotated, including **2-methyl-5,7-dimethoxychromone** (**7**), a chromone derivative with a relative peak intensity 11.15%. It was previously reported from *Hymenophyton flabellatum* and *Penicillium ferraniaense* GE-7, which is inactive against the human lung cancer cell line H1975 [68, 69]. The second compound, **orthosporinin** (**8**), has a relative peak intensity of 5.89%. Compound **8** is a polyketide that was previously isolated from *Ascotricha* sp. ZJ-M-5 was inactive against two human leukaemia cell lines (HL-60 and K562) [70]. The third compound is **boletinin J** (**9**) with a relative peak intensity of 3.70%. Compound **9**, a geranylgeraniol-type diterpenoid isolated from the fruiting bodies of *Boletinus cavipes*, showed no cytotoxicity against macrophage cells [71].

The high peak in RM-$(NH_4)_2SO_4$, with a relative intensity of 12.2%, was putatively annotated as **harzianic acid** (**10**), a polyketide reported from *T. harzianum*. It exhibited antifungal effects against *Pythium irregulare*, *Sclerotinia sclerotiorum*, and *Rhizoctonia solani* [72]. The **2-methyl-5,7-dimethoxychromone** (**7**), with a relative peak intensity of 9.85%, is the second putatively annotated compound in the RM-$(NH_4)_2SO_4$ extract. Then, **trichorozin-IV** (**11**) with a relative intensity of 6.79% was reported from *T. harzianum*. Trichorozin is a peptaibol and is composed of 11 residues, including an amino alcohol. It exhibited voltage-dependent ion-channel-like effects in lipid bilayers [52]. The results of molecular docking using AutoDock Vina for the fungal DHFR are presented in **Table 5**.

The putatively annotated metabolites with the most favourable predicted docking scores against DHFR, with the lowest calculated ΔG_B values, were selected as the most promising inhibitors of DHFR (*ca*DHFR and *cal*DHFR). Based on this criterion, metabolites **7** and **8** showed the most favourable predicted binding interactions with *ca*DHFR, while metabolites **8**, **9**, and **10** showed the most favourable predicted binding interactions with *cal*DHFR. All these putatively annotated metabolites had ΔG_B values below −7 kcal/mol (**Table 5**), suggesting favourable predicted interactions with fungal DHFR, although these predictions do not establish enzyme inhibition. Experimentally, antifungal activity against *C. auris* was observed only for the RM-NaBr and RM-$(NH_4)_2SO_4$ extracts, with IC_{50} values of 35.85 µg/mL and 99.86 µg/mL, respectively. Chemical profiling revealed that metabolites **7**, **8**, and **9** were the putatively annotated metabolites with the highest relative LC-MS peak intensities in the RM-NaBr extract, with relative LC-MS peak intensities of 11.15%, 5.89%, and 3.7%, respectively. In contrast, the RM-$(NH_4)_2SO_4$ extract showed a distinct metabolic profile, with metabolites **10**, **9**, and **11** as the putatively annotated metabolites with the highest relative LC-MS peak intensities, accounting for 12.2%, 9.85%, and 6.79%, respectively. For *C. albicans*, although docking scores were favourable for *C. albicans* DHFR, the corresponding extracts did not show detectable antifungal activity against *C. albicans*. The detailed docking interactions of the putatively annotated metabolites with the most favourable predicted docking scores against *ca*DHFR are presented in (**Table 6** and **Fig. S14)**. Among the metabolites listed in (**Table 5**), putatively annotated metabolites **7** and **8** exhibited the most favourable predicted docking scores against *ca*DHFR. These metabolites were detected in the RM-NaBr and RM-$(NH_4)_2SO_4$ extracts, respectively.

Journal Pre-proof

The crystal structures of bacterial *ec*DHFR (1RG7), fungal *ca*DHFR (8CRH), and *cal*DHFR (4H97) in complex with NADPH show root-mean-square deviations (RMSDs) of 0.937, 0.717, and 1.061 Å, respectively, relative to the bacterial *sa*DHFR-NADPH complex (4FGG). The most conserved sequence regions are located around the substrate- and NADPH-binding sites. Comparison of the substrate-binding subdomain across the four species (*S. aureus*, *E. coli*, *C. auris*, and *C. albicans*) reveals notable differences. Val31 in 4FGG is replaced by Phe31 in 1RG7 and Phe36 in the fungal DHFRs (8CRH and 4H97), enabling potential π-stacking interactions with ligands. Leu20 in 4FGG corresponds to Leu25 in 8CRH, whereas in *E. coli* and *C. albicans*, this residue is substituted by Met20 and Met25, respectively. The Leu→Met substitution, though hydrophobically conservative, appears to abolish antimicrobial activity. The slightly larger and more flexible Met side chain, with its polarizable sulfur, likely perturbs pocket geometry and disrupts precise substrate or catalytic residue positioning, emphasising Leu's critical structural and functional role.

Docking was therefore used exploratorily, as a computational screening tool to assess whether the major putatively annotated metabolites could theoretically fit into the active sites of these enzymes. The results suggested that several putatively annotated metabolites displayed favourable binding poses and predicted interactions with bacterial DHFR (*sa*DHFR and *ec*DHFR), fungal DHFR (*ca*DHFR and *cal*DHFR), and bacterial GyrB (*sa*GyrB and *ec*GyrB). However, given the putative nature of the metabolite annotations, the absence of experimental validation of the docked metabolites and the complexity of crude extracts, these findings should be interpreted cautiously. Docking cannot confirm biological activity, nor can it establish a causal link between predicted binding and the antimicrobial effects observed experimentally. Further biochemical and cellular assays will be required to validate these preliminary observations.

To examine the physicochemical properties, pharmacokinetic and toxicity profiles of the top eleven putatively annotated compounds identified in the YMG-aa, PDA, RM-NaBr and RM-$(NH_4)_2SO_4$ extracts (**Fig. S13** and **Fig. S14**) and the six positive controls, we utilised a freely available online tool called Deep-PK [47](https://biosig.lab.uq.edu.au/deeppk/, accessed on February, 2026). This tool was used to analyse their profiles, and the results are provided in **(Table 4 *Supplementary data)***. In addition, **Table S.3** summarises the physicochemical characteristics as well as the absorption, distribution, metabolism, excretion, and toxicity (ADMET) properties determined for metabolites **3** and **5** on one hand, and for metabolites **7** and **8** on the other, which are our most promising antimicrobial derivatives against *S. aureus* and *C. auris*, respectively. The detailed pharmacokinetic assessment results are presented in the ***Supplementary data***.

3. Conclusions

In conclusion, this study demonstrates the significant impact of the OSMAC strategy on enhancing the chemical diversity of *T. cf. harzianum* fungi by varying fermentation conditions. Several complementary analytical techniques, including dereplication, multivariate analysis, and molecular networking, were employed to compare metabolic profiles and support the selection of putatively annotated candidate metabolites for further bioactivity interpretation. These approaches clearly revealed the variation in metabolic profiles across different cultivation conditions. Additionally, distinct chemical profiles between the agar-based and rice-based

media suggest that the culture composition and incubation duration play an essential role in modulating fungal metabolite synthesis. The antibacterial and antifungal activities of the YMG-aa/PDA and RM-NaBr/RM-$(NH_4)_2SO_4$ extracts against *S. aureus* and *C. auris*, respectively, were experimentally observed, while molecular docking independently predicted favourable interactions with selected bacterial and fungal protein targets. Specifically, tryptanthrin (**3**) and harzianolide (**5**) were putatively annotated in the YMG-aa and PDA extracts, which exhibited antibacterial activity. Both putatively annotated metabolites showed favourable predicted docking interactions with *S. aureus* DHFR and GyrB, respectively. Similarly, 2-methyl-5,7-dimethoxychromone (**7**) and orthosporinin (**8**) were putatively annotated in the RM-NaBr and RM-$(NH_4)_2SO_4$ extracts, which exhibited antifungal activity. Both putatively annotated metabolites showed favourable predicted docking interactions with *C. auris* DHFR. Further studies involving isolation or confirmation of the putatively annotated metabolites, antimicrobial susceptibility testing, and target-specific biochemical assays are required to determine whether these metabolites contribute to the observed extract activities and to investigate their potential mechanisms of action.

Abbreviations

OSMAC: one strain many compounds; LC-HRMS: liquid chromatography -high-resolution mass spectrometry, mm: millimetre; BGCs: biosynthetic gene clusters; CAESAR: Central Asian and European Surveillance of Antimicrobial Resistance, DHFR: Dihydrofolate reductase, Gyr: DNA gyrase, NMR: nuclear magnetic resonance; GNPS: Global Natural Product Social Molecular Network; PDA: potato dextrose agar; °C: Celsius; ITS: Internal Transcribed Spacer, CTAB: cetyltrimethylammonium bromide; DNA: Deoxyribonucleic Acid; ITS1F: Internal Transcribed Spacer 1 Forward; ITS4R: Internal Transcribed Spacer 4 Reverse; PCR: Polymerase Chain Reaction; NCBI: National Center for Biotechnology Information; BLAST: Basic Local Alignment Search Tool; OAT: oatmeal agar, TSA: tryptone soy agar, CZA: Czapek-Dox agar, YMG: yeast malt glucose agar, YMG-aa: yeast malt glucose agar with amino acids; RM: rice grains medium; mL; millilitre; HPLC: High-Performance Liquid Chromatography; min: minute; µL: microlitre; LC/Q-TOF: Liquid Chromatography / Quadrupole Time-of-Flight; ESI: Electrospray Ionization; *m/z*: mass-to-charge ratio; .mgf :Mascot Generic Format; mzXML: Mass Spectrometry Extensible Markup Language; .csv: Comma-Separated Values; ETDG: Experimental-Torsion Distance Geometry; *sa*DHFR: *S. aureus* DHFR; *ec*DHFR: *E. coli* DHFR; GA: genetic algorithm; PLIP: Protein Ligand Interaction Profiler; PCA: Principal component analysis; PLS-DA: partial least squares-discriminant analysis; MS^2:Tandem Mass Spectrometry; Da: Dalton; DMSO: Dimethyl sulfoxide; µg : microgram; h: hour; PC: principal components; 2D: Two-Dimensional; p: p-value; R^2: Coefficient of Determination; VIP: Variable Importance in Projection; Q^2: Predictive Squared Correlation Coefficient; e.g. : for example, HFL1: Fibroblast cell line; KB: Carcinoma in the mouth; BC: Human breast cancer cells; NCI-H187L: Human small cell lung; (Vero) African green monkey kidney fibroblast; kcal/mol : kilocalorie per mole.

Acknowledgements

Amr El-Demerdash is immensely grateful to his home universities, the University of East Anglia (UK) and Mansoura University (Egypt), for the unlimited support inside and outside. We gratefully acknowledge Professor Andrew Truman, from the John Innes Centre for his valuable comments, which enhanced the feasibility and readability of this manuscript.

Data availability

Data will be made available on request.

Authors' contributions (CRediT)

HA and AE contributed to the conceptualisation of the project and the design of the experiments. HA, JA, and ISRS performed the experimental work. HA processed and analysed the data and, together with FP, contributed to software development, computational work, and programming. HA prepared the original manuscript draft. AE supervised the work. AE, SB, AG and MR revised the manuscript. All authors read and approved the final version of the manuscript.

Funding

Hadeel Almagthali is grateful to Taif University for supporting this work through a PhD scholarship. Amr El-Demerdash acknowledges the University of East Anglia for providing funding (Grant No. 60003081AF1) and access to essential research infrastructure. Isabelle SR Storer and Stefan Bidula's funding information is from the Academy of Medical Sciences [SBF008/1046] and the Biotechnology and Biological Sciences Research Council [BB/Y005058/1].

ORCID

Hadeel Almagthali: h.almagthali@uea.ac.uk 0000-0001-9627-4345

Joud Alshammari: j.alshammari@uea.ac.uk

Florbela Pereira: florbela.pereira@fct.unl.pt 0000-0003-4392-4644

Isabelle SR Storer: i.storer@uea.ac.uk 0000-0001-8717-2574

Stefan Bidula: s.bidula@uea.ac.uk 0000-0002-3790-7138

Mostafa E. Rateb: m.rateb@unizwa.edu.om 0000-0003-4043-2687

Journal Pre-proof

A. Ganesan: a.ganesan@uea.ac.uk 0000-0003-4862-7999

Amr El-Demerdash: A.Eldemerdash@uea.ac.uk 0000-0001-6459-295

References

[1] M. A. Fischbach, C. T. Walsh, and J. Clardy, "The evolution of gene collectives: How natural selection drives chemical innovation," *Proceedings of the National Academy of Sciences,* vol. 105, no. 12, pp. 4601-4608, 2008, doi: https://doi.org/10.1073/pnas.0709132105.

[2] D. J. Newman and G. M. Cragg, "Natural products as sources of new drugs over the nearly four decades from 01/1981 to 09/2019," *Journal of natural products,* vol. 83, no. 3, pp. 770-803, 2020, doi: https://doi.org/10.1021/acs.jnatprod.9b01285.

[3] S. D. Bentley *et al.*, "Complete genome sequence of the model actinomycete *Streptomyces coelicolor* A3 (2)," *nature,* vol. 417, no. 6885, pp. 141-147, 2002, doi: https://doi.org/10.1038/417141a.

[4] S. Romano, S. A. Jackson, S. Patry, and A. D. Dobson, "Extending the "one strain many compounds"(OSMAC) principle to marine microorganisms," *Marine drugs,* vol. 16, no. 7, p. 244, 2018, doi: https://doi.org/10.3390/md16070244.

[5] H. B. Bode, B. Bethe, R. Höfs, and A. Zeeck, "Big effects from small changes: possible ways to explore nature's chemical diversity," *ChemBioChem,* vol. 3, no. 7, pp. 619-627, 2002, doi: https://doi.org/10.1002/1439-7633(20020703)3:7<619::AID-CBIC619>3.0.CO;2-9.

[6] M. Han *et al.*, "An endophytic fungus from *Trichoderma harzianum* SWUKD3. 1610 that produces nigranoic acid and its analogues," *Natural Product Research,* vol. 33, no. 14, pp. 2079-2087, 2019, doi: https://doi.org/10.1080/14786419.2018.1486311.

[7] E. L. Ghisalberti and C. Y. Rowland, "Antifungal metabolites from *Trichoderma harzianum*," *Journal of Natural Products,* vol. 56, no. 10, pp. 1799-1804, 1993, doi: https://doi-org.uea.idm.oclc.org/10.1021/np50100a020.

[8] T. Yamada *et al.*, "Tandyukisin, a novel ketoaldehyde decalin derivative, produced by a marine sponge-derived *Trichoderma harzianum*," *Tetrahedron Letters,* vol. 55, no. 3, pp. 662-664, 2014, doi: https://doi.org/10.1016/j.tetlet.2013.11.107.

[9] B. Li *et al.*, "Harzianoic acids A and B, new natural scaffolds with inhibitory effects against hepatitis C virus," *Bioorganic & Medicinal Chemistry,* vol. 27, no. 3, pp. 560-567, 2019, doi: https://doi.org/10.1016/j.bmc.2018.12.038.

[10] S. A. Al-Salihi and F. Alberti, "Genomic based analysis of the biocontrol species *Trichoderma harzianum*: a model resource of structurally diverse pharmaceuticals and biopesticides," *Journal of Fungi,* vol. 9, no. 9, p. 895, 2023, doi: https://doi.org/10.3390/jof9090895.

[11] P. European Centre for Disease and Control, "Antimicrobial resistance in the EU/EEA (EARS-Net) – Annual epidemiological report 2023," ECDC, Stockholm, (accessed on October 2025) 2023. [Online]. Available: https://www.ecdc.europa.eu/en/publications-data/antimicrobial-resistance-eueea-ears-net-annual-epidemiological-report-2023

[12] E. C. f. D. Prevention and Control, "Survey on the epidemiological situation, laboratory capacity and preparedness for *Candidozyma* (*Candida*) *auris*, 2024," ed: ECDC Stockholm, Sweden, 2025.

[13] B. Nammalwar *et al.*, "Inhibition of bacterial dihydrofolate reductase by 6-Alkyl-2, 4-diaminopyrimidines," *ChemMedChem,* vol. 7, no. 11, pp. 1974-1982, 2012, doi: https://doi.org/10.1002/cmdc.201200291.

[14] P. Chawla, G. Teli, R. K. Gill, and R. K. Narang, "An insight into synthetic strategies and recent developments of dihydrofolate reductase inhibitors," *ChemistrySelect,* vol. 6, no. 43, pp. 12101-12145, 2021, doi: https://doi.org/10.1002/slct.202102555.

[15] K. Rajakumari *et al.*, "Comprehensive review of DNA gyrase as enzymatic target for drug discovery and development," *European Journal of Medicinal Chemistry Reports,* vol. 12, p. 100233, 2024, doi: https://doi.org/10.1016/j.ejmcr.2024.100233.

[16] S. M. Ronkin *et al.*, "Discovery of pyrazolthiazoles as novel and potent inhibitors of bacterial gyrase," *Bioorganic & Medicinal Chemistry Letters,* vol. 20, no. 9, pp. 2828-2831, 2010, doi: https://doi.org/10.1016/j.bmcl.2010.03.052.

Journal Pre-proof

[17] N. D. Yuliana, A. Khatib, Y. H. Choi, and R. Verpoorte, "Metabolomics for bioactivity assessment of natural products," *Phytotherapy Research,* vol. 25, no. 2, pp. 157-169, 2011, doi: https://doi.org/10.1002/ptr.3258.

[18] F. M. R. da Silva, G. M. Paggi, F. R. Brust, A. J. Macedo, and D. B. Silva, "Metabolomic strategies to improve chemical information from OSMAC studies of endophytic fungi," *Metabolites,* vol. 13, no. 2, p. 236, 2023, doi: https://doi.org/10.3390/metabo13020236.

[19] A. F. Tawfike, C. Viegelmann, and R. Edrada-Ebel, "Metabolomics and dereplication strategies in natural products," *Metabolomics tools for natural product discovery: methods and protocols,* vol. 1055, pp. 227-244, 2013, doi: https://doi.org/10.1007/978-1-62703-577-4_17.

[20] C. L. Schoch *et al.*, "Nuclear ribosomal internal transcribed spacer (ITS) region as a universal DNA barcode marker for Fungi," *Proceedings of the national academy of Sciences,* vol. 109, no. 16, pp. 6241-6246, 2012, doi: https://doi.org/10.1073/pnas.1117018109.

[21] J. B. Stielow *et al.*, "One fungus, which genes? Development and assessment of universal primers for potential secondary fungal DNA barcodes," *Persoonia-Molecular Phylogeny and Evolution of Fungi,* vol. 35, no. 1, pp. 242-263, 2015, doi: https://doi.org/10.3767/003158515X689135.

[22] D. Godinez-Vidal and S. C Groen. "Optimized CTAB DNA extraction for different tissues v1 protocols." https://dx.doi.org/10.17504/protocols.io.14egn9y8pl5d/v1 (accessed 4-2025.

[23] T. J. White, T. Bruns, S. Lee, and J. Taylor, "Amplification and direct sequencing of fungal ribosomal RNA genes for phylogenetics," *PCR protocols: a guide to methods and applications,* vol. 18, no. 1, pp. 315-322, 1990, doi: https://doi.org/10.1016/B978-0-12-372180-8.50042-1.

[24] N. C. f. B. Information. "GenBank " National Library of Medicine (US), National Center for Biotechnology Information. https://www.ncbi.nlm.nih.gov/genbank/ (accessed June 2025).

[25] S. S. El-Hawary *et al.*, "Bioactive brominated oxindole alkaloids from the Red Sea sponge *Callyspongia siphonella*," *Marine drugs,* vol. 17, no. 8, p. 465, 2019, doi: https://doi.org/10.3390/md17080465.

[26] K. Dührkop *et al.*, "SIRIUS 4: a rapid tool for turning tandem mass spectra into metabolite structure information," *Nature methods,* vol. 16, no. 4, pp. 299-302, 2019, doi: https://doi.org/10.1038/s41592-019-0344-8.

[27] U. Simon Fraser. "The Natural Products Atlas: An Open Access Knowledge Base for Microbial Natural Products." Simon Fraser University. https://www.npatlas.org (accessed September, 2025).

[28] Elsevier. "Reaxys Database." Elsevier. https://www.reaxys.com (accessed September, 2025).

[29] R. M. Salek, C. Steinbeck, M. R. Viant, R. Goodacre, and W. B. Dunn, "The role of reporting standards for metabolite annotation and identification in metabolomic studies," *Gigascience,* vol. 2, no. 1, pp. 2047-217X-2-13, 2013, doi: https://doi.org/10.1186/2047-217X-2-13.

[30] J. D. Holman, D. L. Tabb, and P. Mallick, "Employing ProteoWizard to convert raw mass spectrometry data," *Current protocols in bioinformatics,* vol. 46, no. 1, pp. 13.24. 1-13.24. 9, 2014, doi: https://doi.org/10.1002/0471250953.bi1324s46.

[31] R. Schmid *et al.*, "Integrative analysis of multimodal mass spectrometry data in MZmine 3," *Nature biotechnology,* vol. 41, no. 4, pp. 447-449, 2023, doi: https://doi.org/10.1038/s41587-023-01690-2.

[32] Z. Pang *et al.*, "MetaboAnalyst 6.0: towards a unified platform for metabolomics data processing, analysis and interpretation," *Nucleic acids research,* vol. 52, no. W1, pp. W398-W406, 2024, doi: https://doi.org/10.1093/nar/gkae253.

[33] D. P. Demarque *et al.*, "Mass spectrometry-based metabolomics approach in the isolation of bioactive natural products," *Scientific Reports,* vol. 10, no. 1, p. 1051, 2020, doi: https://doi.org/10.1038/s41598-020-58046-y.

[34] J. J. C. Mingxun Wang, Vanessa V. Phelan, Laura M. Sanchez, Neha Garg, Yao Peng, Don Duy Nguyen et al. , "Sharing and community curation of mass spectrometry data with Global Natural Products Social Molecular Networking.," *Nature biotechnology,* vol. 34, pp. 828–837, 2016, doi: https://doi.org/10.1038/nbt.3597.

[35] P. Shannon *et al.*, "Cytoscape: a software environment for integrated models of biomolecular interaction networks," *Genome research,* vol. 13, no. 11, pp. 2498-2504, 2003, doi: 10.1101/gr.1239303.

[36] H. Mohimani *et al.*, "Dereplication of microbial metabolites through database search of mass spectra," *Nature communications,* vol. 9, no. 1, p. 4035, 2018, doi: https://doi.org/10.1038/s41467-018-06082-8.

Journal Pre-proof

[37] J. A. Kiehlbauch, G. E. Hannett, M. Salfinger, W. Archinal, C. Monserrat, and C. Carlyn, "Use of the National Committee for Clinical Laboratory Standards guidelines for disk diffusion susceptibility testing in New York state laboratories," *Journal of clinical microbiology,* vol. 38, no. 9, pp. 3341-3348, 2000, doi: https://doi.org/10.1128/jcm.38.9.3341-3348.2000.

[38] C. a. L. S. Institute, "Reference Method for Broth Dilution Antifungal Susceptibility Testing of Yeasts.," Clinical and Laboratory Standards Institute, Wayne, M27, 2017. [Online]. Available: https://clsi.org/shop/standards/m27/

[39] C. a. L. S. Institute., "Reference Method for Broth Dilution Antifungal Susceptibility Testing of Filamentous Fungi.," Clinical and Laboratory Standards Institute. , M38, 2017. [Online]. Available: https://clsi.org/shop/standards/m38/

[40] *RDKit: Open-Source Cheminformatics Software*. (2016). RDKit. [Online]. Available: https://www.rdkit.org/

[41] S. Riniker and G. A. Landrum, "Better informed distance geometry: using what we know to improve conformation generation," *Journal of chemical information and modeling,* vol. 55, no. 12, pp. 2562-2574, 2015, doi: https://doi.org/10.1021/acs.jcim.5b00654.

[42] N. M. O'Boyle, M. Banck, C. A. James, C. Morley, T. Vandermeersch, and G. R. Hutchison, "Open Babel: An open chemical toolbox," *Journal of cheminformatics,* vol. 3, no. 1, p. 33, 2011, doi: https://doi.org/10.1186/1758-2946-3-33.

[43] J. Eberhardt, D. Santos-Martins, A. F. Tillack, and S. Forli, "AutoDock Vina 1.2. 0: new docking methods, expanded force field, and python bindings," *Journal of chemical information and modeling,* vol. 61, no. 8, pp. 3891-3898, 2021, doi: https://doi.org/10.1021/acs.jcim.1c00203.

[44] O. Trott and A. J. Olson, "AutoDock Vina: improving the speed and accuracy of docking with a new scoring function, efficient optimization, and multithreading," *Journal of computational chemistry,* vol. 31, no. 2, pp. 455-461, 2010, doi: https://doi.org/10.1002/jcc.21334.

[45] E. F. Pettersen *et al.*, "UCSF Chimera—a visualization system for exploratory research and analysis," *Journal of computational chemistry,* vol. 25, no. 13, pp. 1605-1612, 2004, doi: https://doi.org/10.1002/jcc.20084.

[46] M. F. Adasme *et al.*, "PLIP 2021: expanding the scope of the protein–ligand interaction profiler to DNA and RNA," *Nucleic acids research,* vol. 49, no. W1, pp. W530-W534, 2021, doi: https://doi.org/10.1093/nar/gkab294.

[47] Y. Myung, A. G. de Sá, and D. B. Ascher, "Deep-PK: deep learning for small molecule pharmacokinetic and toxicity prediction," *Nucleic acids research,* vol. 52, no. W1, pp. W469-W475, 2024, doi: https://doi.org/10.1093/nar/gkae254.

[48] I. T. Jolliffe and J. Cadima, "Principal component analysis: a review and recent developments," *Philosophical transactions of the royal society A: Mathematical, Physical and Engineering Sciences,* vol. 374, no. 2065, p. 20150202, 2016, doi: https://doi.org/10.1098/rsta.2015.0202.

[49] S. Xu, C. Bai, Y. Chen, L. Yu, W. Wu, and K. Hu, "Comparing univariate filtration preceding and succeeding PLS-DA analysis on the differential variables/metabolites identified from untargeted LC-MS metabolomics data," (in eng), *Anal Chim Acta,* vol. 1287, p. 342103, Jan 25 2024, doi: 10.1016/j.aca.2023.342103.

[50] A. T. Aron *et al.*, "Reproducible molecular networking of untargeted mass spectrometry data using GNPS," *Nature protocols,* vol. 15, no. 6, pp. 1954-1991, 2020, doi: https://doi.org/10.1038/s41596-020-0317-5.

[51] J. Y. Yang *et al.*, "Molecular networking as a dereplication strategy," *Journal of natural products,* vol. 76, no. 9, pp. 1686-1699, 2013, doi: https://doi.org/10.1021/np400413s.

[52] A. Iida *et al.*, "Fungal metabolities. XVIII. New membrane-modifying peptides, trichorozins I-IV, from the fungus *Trichoderma harzianum*," *Chemical and pharmaceutical bulletin,* vol. 43, no. 3, pp. 392-397, 1995, doi: https://doi.org/10.1248/cpb.43.392.

[53] D. Sinnaeve *et al.*, "Structure and X-ray conformation of pseudodesmins A and B, two new cyclic lipodepsipeptides from Pseudomonas bacteria," *Tetrahedron,* vol. 65, no. 21, pp. 4173-4181, 2009, doi: https://doi.org/10.1016/j.tet.2009.03.045.

[54] D. O. Guimarães *et al.*, "Diketopiperazines produced by endophytic fungi found in association with two *Asteraceae* species," *Phytochemistry,* vol. 71, no. 11-12, pp. 1423-1429, 2010, doi: https://doi.org/10.1016/j.phytochem.2010.05.012.

[55] R. A. A. Khan, S. Najeeb, S. Hussain, B. Xie, and Y. Li, "Bioactive secondary metabolites from *Trichoderma* spp. against phytopathogenic fungi," *Microorganisms,* vol. 8, no. 6, p. 817, 2020, doi: https://doi.org/10.3390/microorganisms8060817.

Journal Pre-proof

[56] S. Bano, N. Bano, V. U. Ahmad, M. Shameel, and S. Amjad, "Marine natural products: 3-formylindole from the red algae *Botryocladia leptopoda*," *Journal of Natural Products,* vol. 49, no. 3, pp. 549-549, 1986, doi: https://doi-org.uea.idm.oclc.org/10.1021/np50045a038.

[57] Q. Yue, C. J. Miller, J. F. White, and M. D. Richardson, "Isolation and characterization of fungal inhibitors from *Epichloë festucae*," *Journal of agricultural and food chemistry,* vol. 48, no. 10, pp. 4687-4692, 2000, doi: https://doi.org/10.1021/jf990685q.

[58] J.-J. Chen, Y.-H. Lin, S.-H. Day, T.-L. Hwang, and I.-S. Chen, "New benzenoids and anti-inflammatory constituents from *Zanthoxylum nitidum*," *Food chemistry,* vol. 125, no. 2, pp. 282-287, 2011, doi: https://doi.org/10.1016/j.foodchem.2010.09.069.

[59] Z. Su, Z. Ma, L. Ye, B. Liu, and S.-X. Qiu, "N-Containing Phytochemicals from the Seeds of *Brucea javanica*," *Chemistry of Natural Compounds,* vol. 53, no. 4, pp. 799-801, 2017, doi: https://doi.org/10.1007/s10600-017-2127-8.

[60] C. Wang, Y. Yang, Z. Mei, and X. Yang, "Cytotoxic compounds from *Laminaria japonica*," *Chemistry of Natural Compounds,* vol. 49, no. 4, pp. 699-701, 2013, doi: https://doi.org/10.1007/s10600-013-0711-0.

[61] J.-l. Zhi *et al.*, "Secondary Metabolites of *Trichoderma spirale*," *Chemistry of Natural Compounds,* vol. 61, no. 4, pp. 821-823, 2025, doi: https://doi.org/10.1007/s10600-025-04771-7.

[62] A. N. Bader, G. L. Salerno, F. Covacevich, and V. F. Consolo, "Native *Trichoderma harzianum* strains from Argentina produce indole-3 acetic acid and phosphorus solubilization, promote growth and control wilt disease on tomato (*Solanum lycopersicum* L.)," *Journal of King Saud University-Science,* vol. 32, no. 1, pp. 867-873, 2020, doi: https://doi.org/10.1016/j.jksus.2019.04.002.

[63] C.-X. Jiang *et al.*, "Isolation, identification, and activity evaluation of chemical constituents from soil fungus *Fusarium avenaceum* SF-1502 and endophytic fungus *Fusarium proliferatum* AF-04," *Journal of agricultural and food chemistry,* vol. 67, no. 7, pp. 1839-1846, 2019, doi: https://doi.org/10.1021/acs.jafc.8b05576.

[64] F. Schindler and H. Zähner, "Stoffwechselprodukte von mikroorganismen," *Arch. Microbiol,* vol. 79, no. 3, pp. 187-203, 1976, doi: https://doi.org/10.1007/BF00446834.

[65] Y. Jahng, "Progress in the studies on tryptanthrin, an alkaloid of history," *Archives of pharmacal research,* vol. 36, no. 5, pp. 517-535, 2013, doi: https://doi.org/10.1007/s12272-013-0091-9.

[66] S. Rebuffat, C. Goulard, and B. Bodo, "Antibiotic peptides from *Trichoderma harzianum:* harzianins HC, proline-rich 14-residue peptaibols," *Journal of the Chemical Society, Perkin Transactions 1,* no. 14, pp. 1849-1855, 1995, doi: 10.1039/P19950001849.

[67] F. Cai *et al.*, "Harzianolide, a novel plant growth regulator and systemic resistance elicitor from *Trichoderma harzianum*," *Plant Physiology and Biochemistry,* vol. 73, pp. 106-113, 2013, doi: https://doi.org/10.1016/j.plaphy.2013.08.011.

[68] M. Toyota, I. Omatsu, J. Braggins, and Y. Asakawa, "Pungent aromatic compound from New Zealand Liverwort *Hymenophyton flabellatum*," *Chemical and Pharmaceutical Bulletin,* vol. 57, no. 9, pp. 1015-1018, 2009, doi: https://doi.org/10.1248/cpb.57.1015.

[69] Y. Wang *et al.*, "Chemical constituents of *Penicillium ferraniaense* GE-7 and their cytotoxicities," *Natural Product Research,* vol. 39, no. 14, pp. 3915-3922, 2025, doi: https://doi.org/10.1080/14786419.2024.2324113.

[70] J.-L. Zhang *et al.*, "From macrocyclic to linear and further: naturally degradable polyesters from the fungus *Ascotricha* sp. ZJ-M-5," *Tetrahedron,* vol. 72, no. 32, pp. 4895-4901, 2016, doi: https://doi.org/10.1016/j.tet.2016.06.062.

[71] T. Kamo, K. Sato, K. Sen, H. Shibata, and M. Hirota, "Geranylgeraniol-type diterpenoids, boletinins A− J, from *Boletinus cavipes* as inhibitors of superoxide anion generation in macrophage cells," *Journal of natural products,* vol. 67, no. 6, pp. 958-963, 2004, doi: https://doi.org/10.1021/np030535g.

[72] F. Vinale *et al.*, "Harzianic acid, an antifungal and plant growth promoting metabolite from *Trichoderma harzianum*," *Journal of Natural Products,* vol. 72, no. 11, pp. 2032-2035, 2009, doi: https://doi.org/10.1021/np900548p.

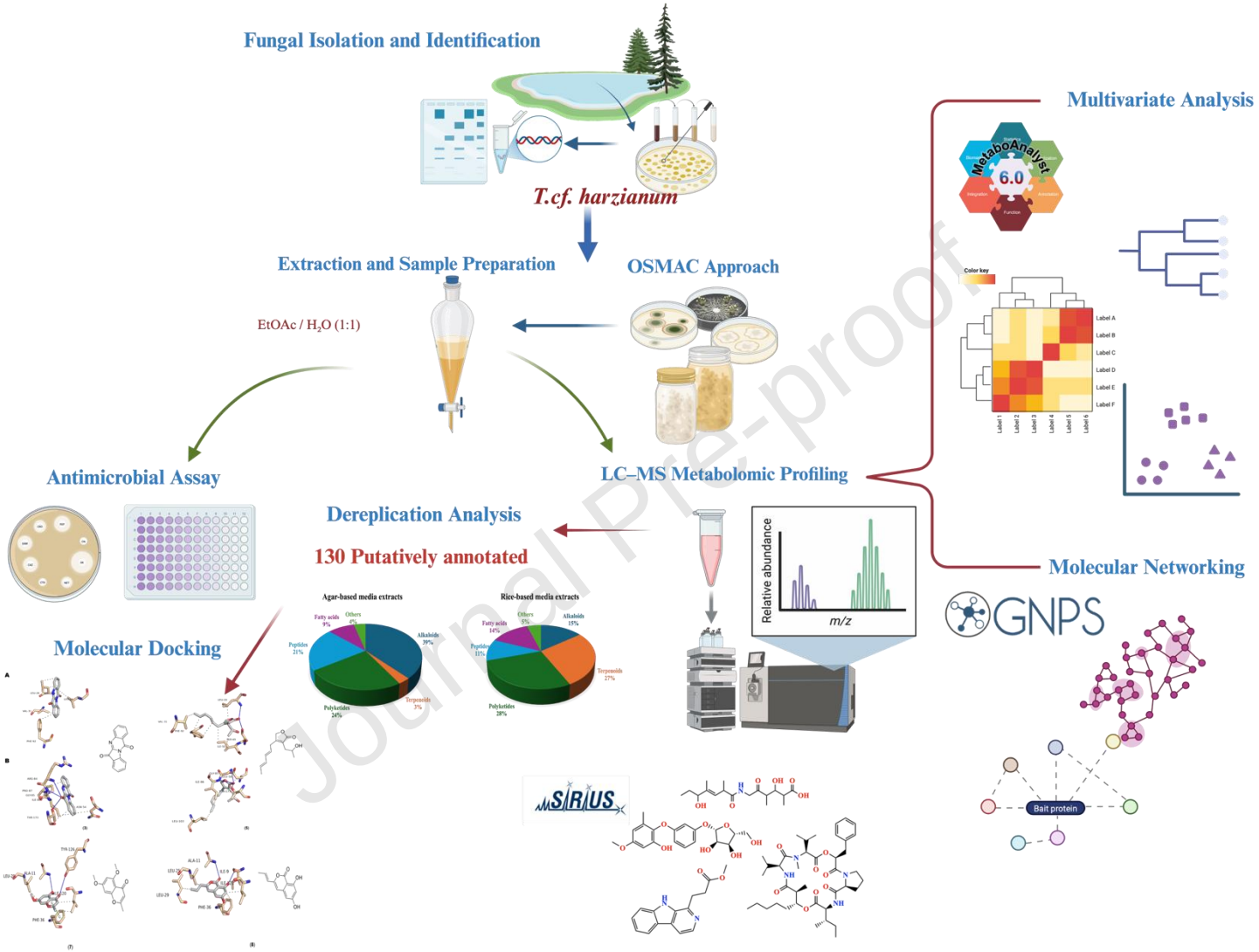
Journal Pre-proof

Highlights

- This study assesses the OSMAC approach on *Trichoderma cf. harzianum* metabolites.
- Using Q-ToF-LC-HR-MS and molecular networking, 130 LC-MS features were putatively annotated.
- Ten different culture conditions significantly enhance fungal chemical diversity.
- Extracts show antimicrobial activity against *S. aureus and C. auris.*
- Molecular docking suggests the most favourable predicted docking scores against DHFR and DNA gyrase B.

Graphical abstract

Journal Pre-proof



Journal Pre-proof

Fig.1: HPLC profile of different extracts. **a**) Agar-based media. **b**) Rice-based media at 254 nm.

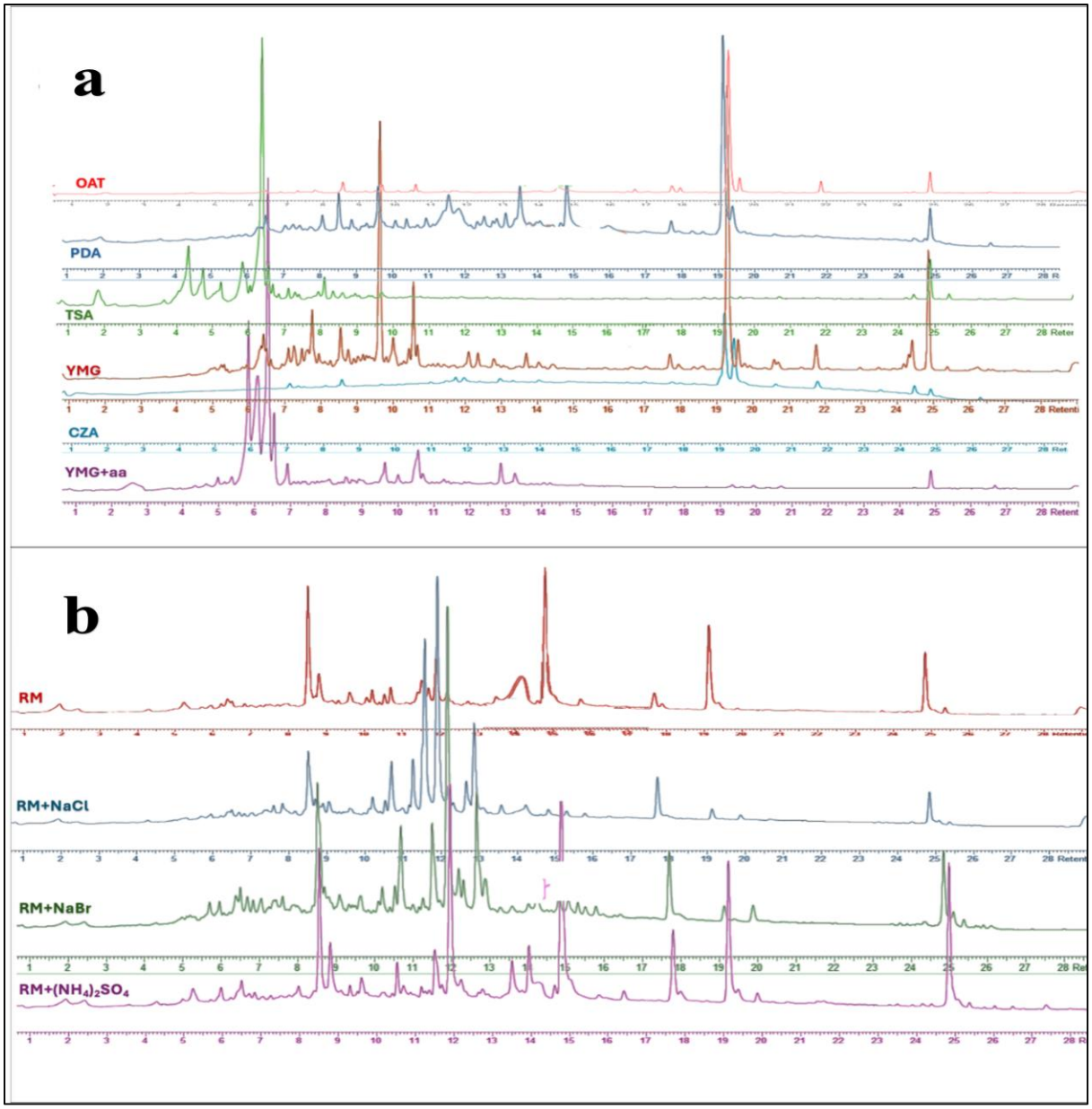
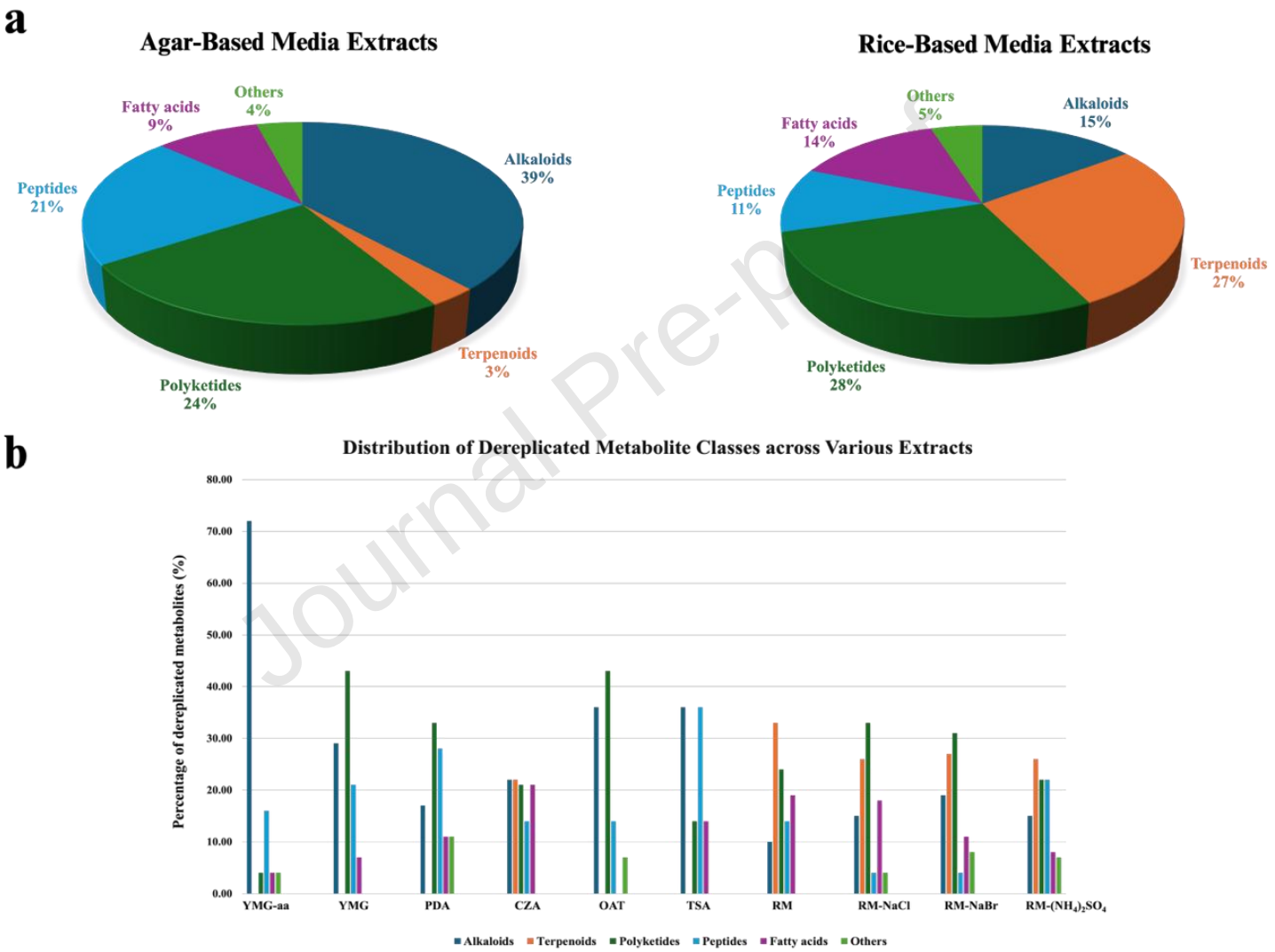


Fig.2: Chemical class distribution of putatively annotated metabolites from SIRIUS detected under different cultivation conditions. (**a**) Pie chart showing the relative % of different chemical classes in agar-based and rice-based media extracts. (**b**) Bar chart showing the relative % distribution of metabolite classes across individual culture media.



Journal Pre-proof

Fig.3: Metabolomics multivariate analysis: **a**) 2D Score plots of PCA, **b**) HCA plot shown as a dendrogram; **c**) k-means clustering analysis, **d**) PLS-DA scores plot, **e**) VIP score plot of PLS-DA, **f**) Heatmap of the most significantly variable 25 features among the samples corresponding to the ten different extracts.

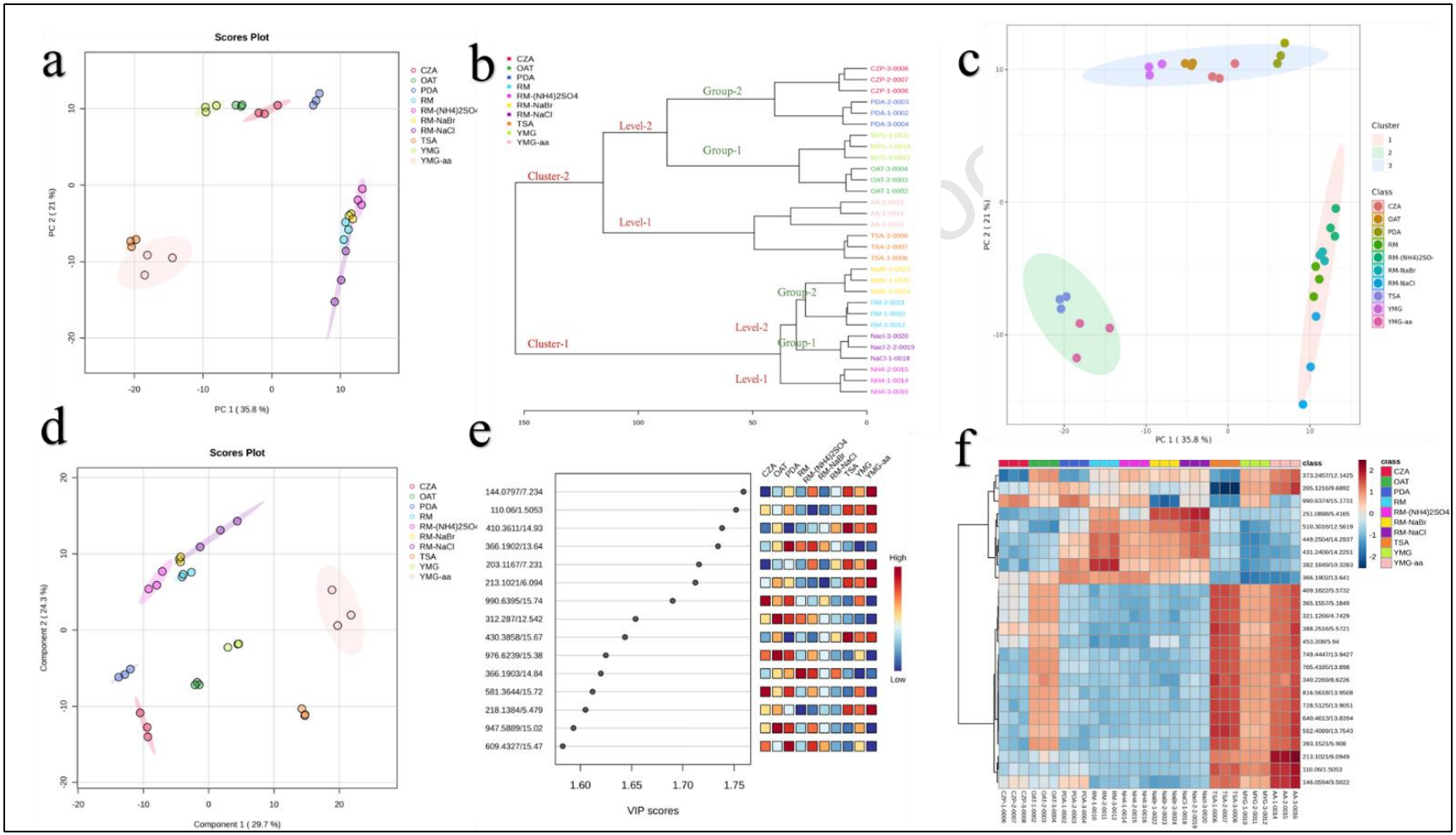
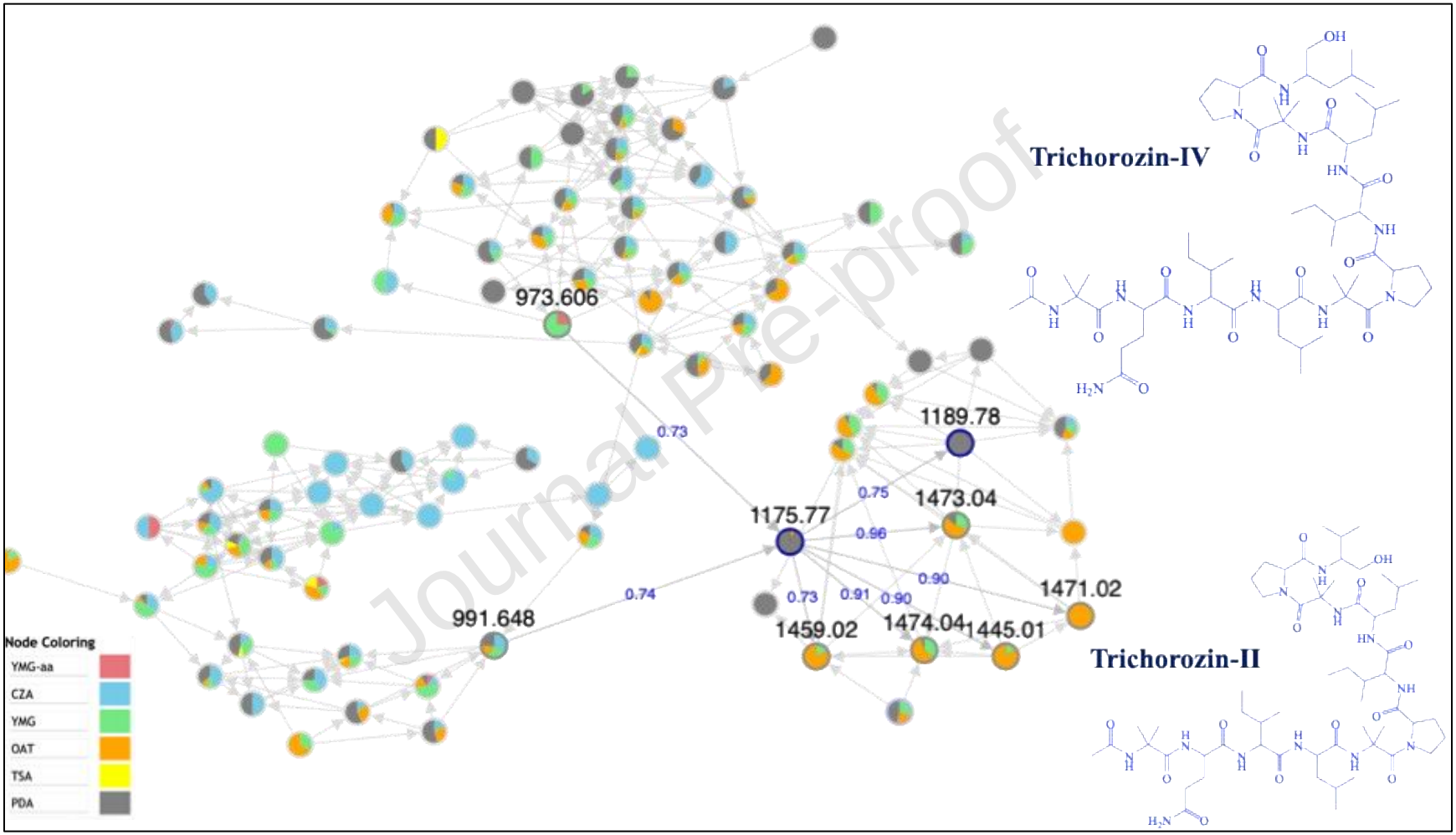
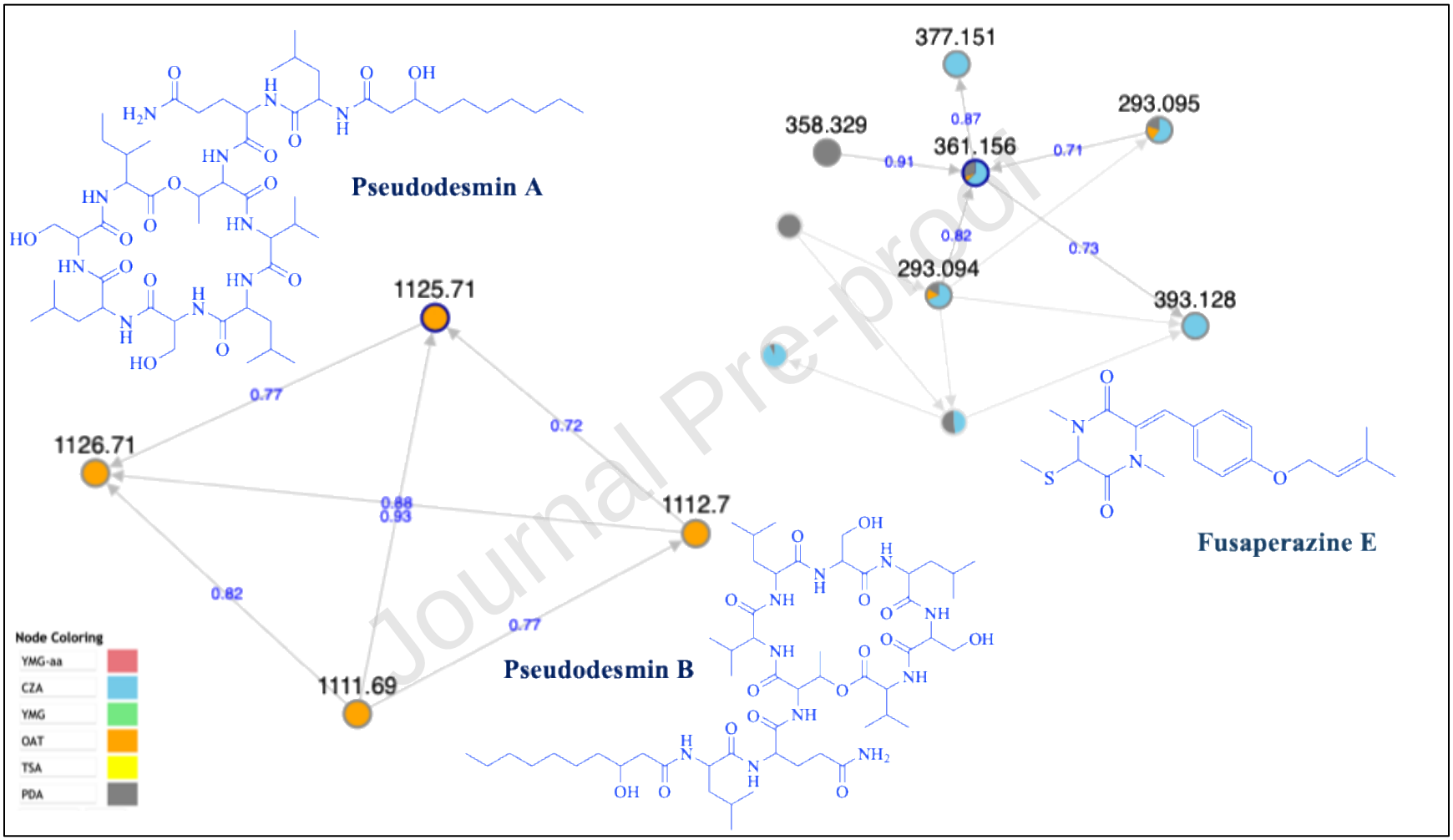


Fig.4. A zoomed-in, annotated cluster molecular network, with nodes from the selected molecular class labelled with parent mass, is displayed as pie charts showing the distribution of ion intensities; annotated cluster **3** molecular network of the agar-based media extracts; **b**) annotated cluster **27** and **47** molecular network of the agar-based media extracts; **c**) annotated cluster **3** molecular network of the rice-based media extracts.



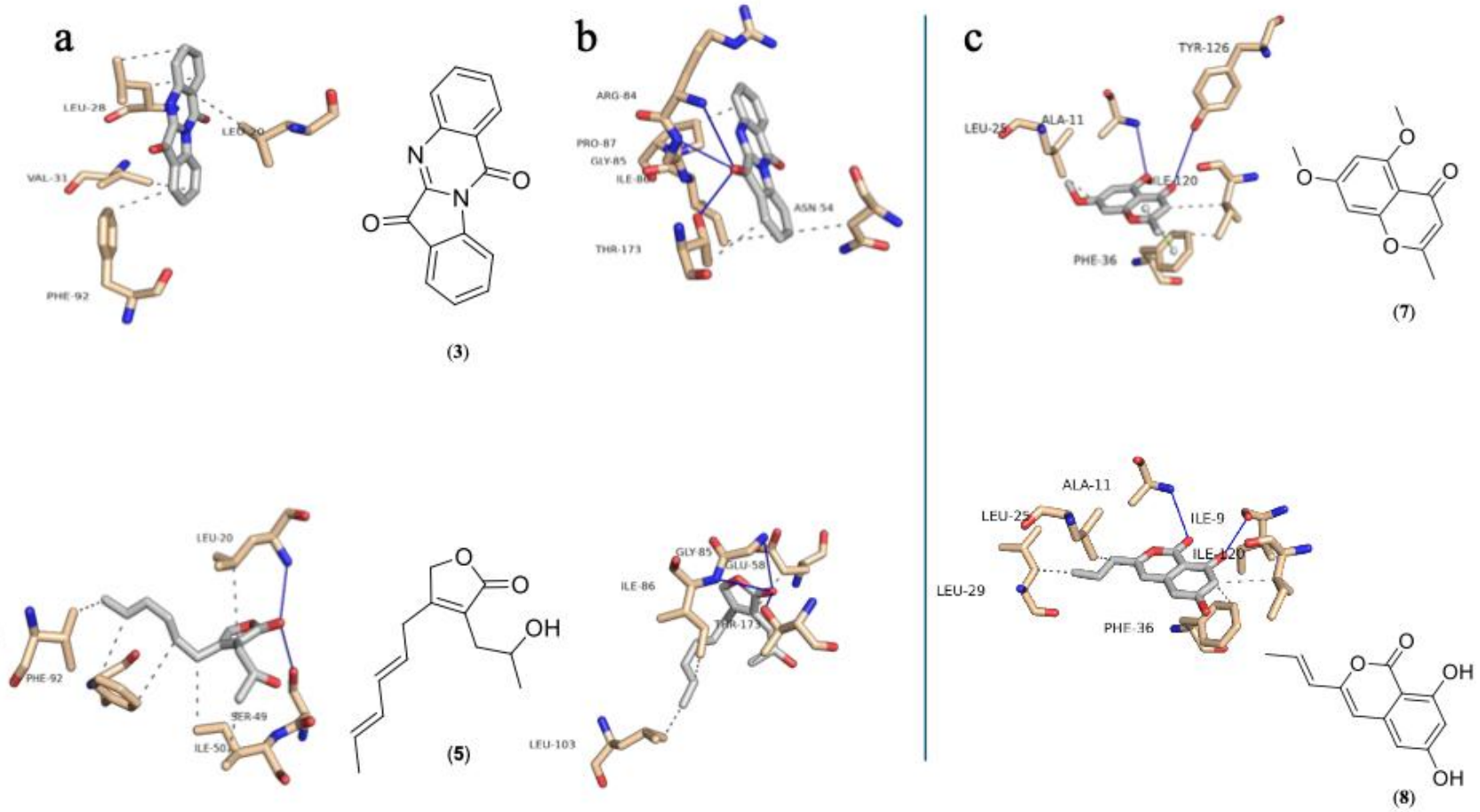
Journal Pre-proof

Fig.5. A zoomed-in, annotated cluster molecular network, with nodes from the selected molecular class labelled with parent mass, is displayed as pie charts showing the distribution of ion intensities; annotated cluster **27** and **47** molecular networks of the agar-based media extracts.



Journal Pre-proof

Fig.6 Interaction profiles of the best-docked poses of metabolites **3** and **5** for: **a**) *sa*DHFR; **b**) *sa*GyrB; **c**) Interaction profiles of the best-docked poses of metabolites **7** and **8** for *ca*DHFR. The hydrophobic interactions are depicted as black dashed lines, the hydrogen bonds as blue continuous lines, and π stacking interactions as green dashed lines.



Journal Pre-proof

Table 1. SIRIUS-based molecular formula predictions for the 15 VIP LC-MS features selected by PLS-DA.

Feature m/z	RT (min)	Molecular Formula	Adduct	Median Mass Error (ppm)	SIRIUS Score (%)
144.0797	7.23	$C_{10}H_9N$	$[M+H]^+$	-2.2	100.0
410.3611	14.93	$C_{25}H_{47}NO_3$	$[M+H]^+$	+0.6	100.0
213.1021	6.09	$C_{13}H_{12}N_2O$	$[M+H]^+$	-0.7	98.7
990.6395	15.74	$C_{47}H_{83}N_{13}O_{10}$	$[M+H]^+$	-2.2	97.4
312.287	12.54	$C_{19}H_{37}NO_2$	$[M+H]^+$	-0.01	99.9
430.3858	15.67	$C_{25}H_{51}NO_4$	$[M+H]^+$	+1.1	99.9
366.1903	14.84	$C_{19}H_{27}NO_6$	$[M+H]^+$	-2.0	99.9
581.3644	15.72	$C_{28}H_{48}N_6O_7$	$[M+H]^+$	-0.3	99.9
218.1384	5.48	$C_{11}H_{15}N_5$	$[M+H]^+$	+0.7	99.9
947.5889	15.02	$C_{44}H_{80}N_{10}O_{11}$	$[M+Na]^+$	-0.7	99.9
609.4327	15.47	$C_{36}H_{56}N_4O_4$	$[M+H]^+$	-1.9	83.4

Table 2. SIRIUS-based molecular formula predictions for the top 25 LC-MS features selected from the heatmap analysis.

Feature (m/z)	RT (min)	Molecular Formula	Adduct	Median Mass Error (ppm)	SIRIUS Score (%)

373.2457	12.14	$C_{17}H_{32}N_4O_5$	$[M+H]^+$	+0.7	100.0
205.1216	9.69	$C_{13}H_{16}O_2$	$[M+H]^+$	+0.5	99.97
990.6374	15.17	$C_{47}H_{83}N_{13}O_{10}$	$[M+H]^+$	-2.2	97.4
510.3016	12.56	$C_{22}H_{43}N_3O_{10}$	$[M+H]^+$	+1.3	96.8
449.2504	14.29	$C_{20}H_{36}N_2O_9$	$[M+H]^+$	+0.1	76.3
431.2406	14.23	$C_{23}H_{36}O_6$	$[M+Na]^+$	+0.2	91.2
382.1849	10.33	$C_{19}H_{27}NO_7$	$[M+H]^+$	+1.1	99.4
366.1902	13.64	$C_{19}H_{27}NO_6$	$[M+H]^+$	-2.0	99.99
321.1266	4.74	$C_{13}H_{22}N_4O_3$	$[M+K]^+$	-0.4	73.9
388.2516	5.57	$C_{17}H_{33}N_5O_5$	$[M+H]^+$	+0.6	100.0
749.4447	13.94	$C_{35}H_{62}N_6O_{10}$	$[M+Na]^+$	+1.3	99.7
705.4185	13.90	$C_{35}H_{56}N_6O_9$	$[M+H]^+$	+4.1	99.9
728.5125	13.91	$C_{43}H_{69}NO_8$	$[M+H]^+$	-1.6	77.6
640.4613	13.84	$C_{33}H_{61}N_5O_7$	$[M+H]^+$	+0.8	89.1
552.4089	13.75	$C_{29}H_{53}N_5O_5$	$[M+H]^+$	-0.1	100.0
213.1021	6.09	$C_{13}H_{12}N_2O$	$[M+H]^+$	-0.7	98.7
146.0594	3.50	C_9H_7NO	$[M+H]^+$	+0.1	99.8

Journal Pre-proof

Table 3. Calculated free binding energies (ΔG_B, in kcal/mol) established upon docking the top six putatively annotated metabolites (**1-6**) from (YMG-aa) and (PDA) and the four positive controls against DHFR and GyrB.

Metabolites	DG_B (kcal/mol)			
	DHFR		GyrB	
	***sa*DHFR**[1]	***ec*DHFR**[2]	***sa*Gyr**[1]	***ec*Gyr**[2]
1	-5.734	-6.841	-5.216	-5.871
2	-6.366	-7.347	-5.8	-6.592
3	-7.829	-7.998	-7.832	-9.053
4	-6.927	-7.013	-5.95	-4.156
5	-6.794	-7.435	-6.385	-7.28
6	-7.074	-6.856	-5.937	-8
PC[3]	-7.983[4]	-9.011[5]	-6.299[6]	-9.708[7]

[1]From *Staphylococcus aureus*. [2]From *E. coli*. [3]Positive Control. [4]Propyl-DAP 2-methylprop-1-en-1-yl-dihydrophthalazine. [5]Methotrexate. [6]4-Methyl-5-[3-(methylsulfanyl)-1H-pyrazol-5-yl]-2-thiophen-2-yl-1,3-thiazole. [7]Prop-2-yn-1-yl {[5-(4-piperidin-1-yl-2-pyridin-3-yl-1,3-thiazol-5-yl)-1H-pyrazol-3-yl] methyl} carbamate.

Table 4. Docking interactions of the most favourable predicted docking scores against *sa*DHFR and *sa*GyrB and the two positive controls.

Metabolite	Source	Interaction		
		Hydrophobic residues	H-bond residues	Other residues
3	*sa*DHFR	Leu20, Leu28(2), Val31, Phe92	---	---
4		Pro25, Leu28(2), Val31, Leu54, Pro55	Lys32, Arg57	---
5		Leu20, Val31, Ile50(2), Phe92(2)	Leu20, Ser49	---
6		Leu28, Val31(2), Ile50, Leu54, Phe92(2)	Arg57	p-Stacking: Phe92
PC[1]		Leu20, Ile50(2), Leu54(2), Pro55, Phe92(2)	Lys52	Salt bridges: Asp27
3	*sa*GyrB	Asn54, Ile86, Pro87, Thr173	Arg84, Gly85, Thr173	---
5		Glu58, Ile86(2), Leu103, Thr173	Gly85, Ile86, Thr173	---
PC[2]		Ile86, Pro87	Asn54, Glu58	p-Cation: Arg84

[1]Positive control, propyl-DAP 2-methylprop-1-en-1-yl-dihydrophthalazine. [2]Positive control, 4-methyl-5-[3-(methylsulfanyl)-1H-pyrazol-5-yl]-2-thiophen-2-yl-1,3-thiazole.

Table 5. Calculated free binding energies (ΔG_B, in kcal/mol) established when the top five putatively annotated metabolites (**7**–**11**) identified from RM-NaBr and RM-$(NH_4)_2SO_4$ were docked against fungal DHFR, along with the two positive controls.

DHFR	DG_B (kcal/mol)					
	Metabolites					
	7	**8**	**9**	**10**	**11**	**PC**[3]
*ca*DHFR[1]	-7.013	-7.302	-6.153	-5.25	-5.7	-6.273[4]
*cal*DHFR[2]	-6.474	-7.58	-8.361	-7.549	-7.462	-10.56[5]

[1]From *Candidozyma auris*. [2]From *Candida albicans*. [3]Positive Control. [4]5-(4-chlorophenyl)-6,6-dimethyl-1,4-dihydro-1,3,5-triazine-2,4-diamine. [5]5-[(3*R*)-3-(5-methoxy-4'-methylbiphenyl-3-yl) but-1-yn-1-yl]-6-methylpyrimidine-2,4-diamine.

Journal Pre-proof

Table 6. Docking interactions of the most favourable predicted docking scores against *ca*DHFR and the positive control.

Metabolite	Source	Interaction		
		Hydrophobic residues	H-bond residues	Other residues
7	*ca*DHFR	Leu25, Ile120(2)	Ala11, Tyr126	p-Stacking: Phe36
8		Leu25, Leu29, Phe36, Ile120	Ile9, Ala11	---
PC[1]		Phe36, Thr57, Ile120	Ala11	Salt bridges: Glu32. p-Stacking: Phe36

[1]Positive control, 5-(4-chlorophenyl)-6,6-dimethyl-1,4-dihydro-1,3,5-triazine-2,4-diamine.

Journal Pre-proof

Declaration of Interest Statement

☒ The authors declare that they have no known competing financial interests or personal relationships that could have appeared to influence the work reported in this paper.

Journal Pre-proof